AD NUMBER
AD381544
CLASSIFICATION CHANGES
TO: **unclassified**
FROM: **confidential**
LIMITATION CHANGES
TO: **Approved for public release, distribution unlimited**
FROM: **Controlling DoD Organization: Office of Naval Research, Arlington, VA 22217**
AUTHORITY
Office of Naval Research ltr dtd 4 May 1977; Office of Naval Research ltr dtd 4 May 1977

SECURITY MARKING

The classified or limited status of this report applies to each page, unless otherwise marked.
Separate page printouts MUST be marked accordingly.

THIS DOCUMENT CONTAINS INFORMATION AFFECTING THE NATIONAL DEFENSE OF THE UNITED STATES WITHIN THE MEANING OF THE ESPIONAGE LAWS, TITLE 18, U.S.C., SECTIONS 793 AND 794. THE TRANSMISSION OR THE REVELATION OF ITS CONTENTS IN ANY MANNER TO AN UNAUTHORIZED PERSON IS PROHIBITED BY LAW.

NOTICE: When government or other drawings, specifications or other data are used for any purpose other than in connection with a definitely related government procurement operation, the U. S. Government thereby incurs no responsibility, nor any obligation whatsoever; and the fact that the Government may have formulated, furnished, or in any way supplied the said drawings, specifications, or other data is not to be regarded by implication or otherwise as in any manner licensing the holder or any other person or corporation, or conveying any rights or permission to manufacture, use or sell any patented invention that may in any way be related thereto.

DOCUMENT 97649

DETECTION OF OPTICAL SIGNATURE OF SUBMARINES BY LASER TECHNIQUES (U)

TECHNICAL REPORT

CONTRACT NOnr 3358(00)

Office of Naval Research
Department of the Navy
Washington 25, D.C.

Author: L. M. Vallese, Senior Scientist

ITT FEDERAL LABORATORIES
a division of International Telephone and Telegraph Corporation
500 Washington Avenue Nutley, New Jersey 07110

NOVEMBER 1966

TABLE OF CONTENTS

LIST OF ILLUSTRATIONS

ABSTRACT

Methods for the detection of the optical signature of submarines by means of laser techniques are discussed. The principal approaches considered are those based on the optical doppler effect and on the optical matched filtering. The experimental results obtained in the course of the investigation are presented and are discussed from the point of view of the feasibility of the techniques. It is shown that, while it is difficult to extend the optical doppler method from laboratory to field operation, the optical matched-filtering method lends itself to the design of simple instrumentation for the detection of the optical signature in real time.

ACKNOWLEDGMENT

The work described in this report was developed as one of the Project Tasks under Contract NOnr 3358; the report describes the results obtained up to June 30, 1966. The investigation was conducted at ITT Federal Laboratories under the direction of Dr. L. M. Vallese, Senior Scientist and Head of the Physical Electronics Department. Other contributors were Messrs. J. Bula, A. M. Passalaqua, F. Dynda.

The support of the Office of Naval Research (Dr. A. Shostak, Head of the Electronics Branch) is gratefully acknowledged.

1. INTRODUCTION

The following report covers work of investigation of techniques for the detection of submarines by means of laser techniques. The work was conducted under Contract NOnr 3358, and was completed in June 1966.

The investigation has been directed to the detection of the "optical signature" of submarines. The equilibrium configuration of the sea-air interface is determined by the elastic waves propagated within the water and corresponds to a surface where the pressure equals that of the atmosphere; thus, any perturbation caused by submarines, vessels, as well as winds, etc., contributes to the resultant configuration. In particular, a submarine in motion constitutes a distinct source of such waves which produces surface "signatures" such as wakes and modifications of the mean slopes of water waves.

Visual as well as radar detection of submarine wakes have been demonstrated; however, these means of detection have not proven sufficiently practical, sensitive, or reliable. It appears that, by recourse to coherent optical techniques, a greatly enhanced sensitivity may be obtained, thus opening the way to the design of field equipment with suitable operational characteristics.

In the following, two approaches to the problem of detection of the optical signature by means of lasers will be described. The first is based on the measurement of optical frequency shifts produced by doppler effects, and the second is based on the use of optical intensity scatter as well as optical matching filters and electronic systems of signal-to-noise enhancement. We precede the treatment with a review of the basic theories of hydrodynamics which provide a quantitative description of the optical-signature phenomena at the sea surface.

2. PRINCIPLES OF HYDRODYNAMICS

The analysis of the sea-surface waves has been the subject of extensive investigations; the basic theories have been developed in hydrodynamics and are associated with the names of Lagrange, Stokes, Kelvin, Lamb, to name only a few. In particular, Kelvin has provided a beautiful description of the physical phenomena of wakes created by ships in motion.

The equations of hydrodynamics may be expressed either with reference to the motion of individual fluid particles (Lagrange form), or with reference to the velocity distribution at fixed points in the medium, as functions of time (Euler form). In general, indicating with ρ the density of water, with p the pressure, with $\bar{F}$ the body force, with $\bar{a}$ the acceleration, and with $\bar{v}$ the velocity, one can write the following general equations:

Equation of Motion	$\frac{-1}{\rho} \text{ grad } p + \bar{F} = \bar{a}$	(1)
Equation of Continuity	$\text{div } \bar{v} = 0$	(2)
Equation of Irrotational Flow	$\text{curl } \bar{v} = 0$	(3)

As a result of application of Equation 3, one can express the velocity vector as the gradient of a single-valued scalar potential function ϕ (x, y, z, t) ; i.e.,

$$\bar{v} = \text{grad } \phi \qquad (4)$$

This relation is very important, because it reduces the study of the vector quantity $\bar{v}$ to that of a scalar function; substituting Equation 4 into Equation 2, one has:

$$\nabla^2 \phi = 0 \qquad (5)$$

i.e., the function ϕ is obtained as solution of the linear scalar Laplace's equation.

Substitution of Equation 4 into Equation 1 provides a representation of the motion in terms of ϕ (Eq. of Bernoulli); for example, the equation of motion of a fluid particle subject to the force of gravity is expressed as follows:

$$\frac{d\phi}{dt} + \frac{1}{2}(u^2 + v^2 + w^2) + \frac{p}{\rho} + gy = c(t) \qquad (6)$$

where u, v, w are scalar velocity components, and $c(t)$ is a function derived from time-dependent external forces.

Thus, the solution of the problems of hydrodynamics is carried out determining first the scalar potential function ϕ from Equation 5, and secondly the velocity components u, v, w from Equation 6.

The conditions at the boundaries of the sea medium are of two types: a) those corresponding to the sea bottom, where the surface is fixed and therefore the normal component of the velocity is zero; these boundary conditions are expressed as follows:

$$\frac{d\phi}{dn} = 0 \quad \text{on} \quad S \tag{7}$$

b) those corresponding to the sea-air interface, where the vertical component of the acceleration is zero, because the surface is "free" and assumes a form such that $\bar{a} = 0$. Referring to a Cartesian reference system of axes, with origin at the undisturbed water surface and y-axis directed vertically upwards, the latter boundary condition is expressed as follows:

$$\phi_x \eta_x - \phi_y + \phi_z \eta_z + \eta_t = 0 \quad \text{on} \quad S \tag{8}$$

where ϕ_x, ϕ_y, ϕ_z, η_x, η_z, η_t are partial derivatives with respect to the variables x, y, z, t, and

$$y = \eta(x, z, t) \tag{9}$$

is the equation of the "free" surface S.

The above relationships provide the mathematical means for the determination of the propagation of waves and of the configuration of the sea surface. For example, progressive surface gravity waves, where the gravity force is predominant over the surface tension, are represented with the following velocity potential function:

$$\phi = A \cos h\, \beta(y+h) \cos(\beta x \pm \sigma t + \alpha) \tag{10}$$

where h is the depth of the sea, α is a phase angle, and the quantities β and σ have the following significance:

$$\beta = \frac{2\pi}{\lambda}$$
$$\sigma^2 = g\beta \tan h\, \beta h \qquad (11)$$

If the depth h is very large,

$$\sigma^2 = g\beta \qquad (12)$$

The velocity component along the x direction is expressed as follows:

$$v = u = \frac{\sigma}{\beta} = \sqrt{\frac{g}{\beta}} = \sqrt{\frac{g\lambda}{2\pi}} \qquad (13)$$

More generally, if the surface tension T is considered, the latter relation is expressed as follows:

$$v = \sqrt{\frac{2\pi T}{\lambda g} + \frac{g\lambda}{2\pi}} \qquad (14)$$

The function 14 is represented graphically in Fig. 1 versus the wavelength λ ; it is noted that the velocity changes markedly depending on whether the surface tension T or the gravity g is the restoring force. The former case corresponds to capillary waves, and the latter to gravity waves.

The frequency of oscillation of the waves is computed with the familiar relationship $\lambda f = v$, and thus varies with the wavelength, with the following functional relationship:

$$f = \sqrt{\frac{2\pi T}{\rho\lambda^3} + \frac{g}{2\pi\lambda}} \qquad (15)$$

With reference to Fig. 1, it is noted that a minimum velocity of 20 - 30 cm/sec occurs in correspondence of $\lambda = 1 \div 2$ cm ; capillary waves display wavelength values less than 1 cm , and frequency larger than $10 \div 15$ c/sec. Schooley has pointed out[1,2,3] that, while small waves (both capillary and gravity type) have approximately sinusoidal profiles, large waves of gravity type have a modified trochoidal shape, sharper near the crests and flatter in the troughs, while large waves of capillary type have sharp troughs and wide crests and, in general, larger average slope than gravity waves (Fig. 2). The

surface slope also depends upon the wind and statistically is peaked and skewed in the down-wind direction (compared to a Gaussian distribution - Fig. 3).

As far as the wake pattern is concerned, it is sufficient to summarize the results derived from Kelvin[4]. Indicating with C the course of a ship, and assuming that the origin of the coordinates axes moves with the ship (Fig. 4), the curve C may be represented parametrically with the equations:

$$\begin{aligned} x_1 &= x_1(t) \\ z_1 &= z_1(t) \end{aligned} \qquad 0 \leq t \leq T \tag{16}$$

where t is the time variable. Kelvin has shown that the vertical profile of the sea surface $y = \eta(z, t)$ may be expressed as an integral:

$$\eta(z, t) = k_o \int_0^T \frac{t^3}{r^4} \sin \frac{g t^2}{4r} \, dt \tag{17}$$

where r yields the distance between a point (x,z) and a point (x_1, z_1) on the course; i.e.,

$$r = \sqrt{(x - x_1)^2 + (z - z_1)^2} \tag{18}$$

The integral (17) was computed approximately by the method of "stationary phase". Loci of constant phase, for a number of phase values differing by 2π, are shown in Fig. 5 for the case of a straight course at constant speed and, in Fig. 6, for the case of a circular course at constant speed. In the former example (Fig. 5), the curves are represented in terms of the angle θ (Fig. 4), with the following equation:

$$\begin{aligned} x &= \frac{a}{2} (2 \cos \theta - \cos^3 \theta) \\ z &= \frac{a}{2} \cos^2 \theta \sin \theta \end{aligned} \tag{19}$$

where a is a parameter depending upon the velocity and having the dimensions of length. These curves constitute two systems of waves, respectively divergent and transverse, which cover a V-shaped region called the "influence region", and join at the boundary of such region; the points of junction are cusps and correspond to the condition $\theta = \theta^*$, where

$$3 \sin^2 \theta^* = 1 \tag{20}$$

It can be shown that in first approximation the disturbance at a point $P(x,y)$ is determined only by certain discrete points Q_i on the ship course C given by the relation:

$$r = \frac{1}{2} c t \cos \theta \tag{21}$$

where c and t are respectively speed and time; in fact, the contributions from all other points cancel out because of mutual interference. The points Q are called "influence points"; for a given point Q, one can compute from (21) the values of the coordinates (r, θ) of points P for which Q is the influence point. Such points P are found on a circle (Fig. 6) with diameter tangent to the course C at Q, where Q is on the circumference. This property permits one to construct geometrically the outline of the region in which the disturbance caused by the ship's motion is confined. For example, in Fig. 7, the case of a straight-path course is shown; circles of radius 1/4 c t are drawn at various points Q and delimit by envelope the "wake" boundaries. We see that, if the speed c is constant, the boundaries are two straight lines with semiangle $\tau = 19°28'$ independent of the speed c. The importance of this result for application to detection is obvious.

It can be shown that the curves of constant phase of a wake are orthogonal to the lines drawn back to the influence points. This is shown graphically in Fig. 8 and is demonstrated by differentiation of Equation 19. One finds:

$$\frac{dx}{d\theta} = -\frac{a}{2}(3 \sin^2 \theta - 1) \sin \theta$$

$$\frac{dz}{d\theta} = \frac{a}{2}(3 \sin^2 \theta - 1) \cos \theta \tag{22}$$

and

$$\frac{dz}{dx} = -\frac{1}{\tan \theta} \tag{23}$$

From Equations 22 and 23, it is also found that the points θ^* defined by Equation 20 are singular and correspond to the cases in which the influence points of the divergent and transversal constant-phase waves coincide.

Finally, the amplitudes of the wake waves can be computed approximately, although laboriously. In general, it is found that they are inversely proportional to the square root of the distance from the ship.

3. DETECTION OF SIGNATURE BY DOPPLER FREQUENCY MEASUREMENTS

The doppler effect may be used to measure the relative velocity of a target with respect to observer as a function of the shift of the frequency of a reflected electromagnetic wave as seen by an observer. Assuming that the component of velocity along the path of propagation and reflection is v, the frequency f of electromagnetic wave scattered from the target is:

$$f' = f \frac{1 - v/c}{\sqrt{1 - \left(\frac{v}{c}\right)^2}} \tag{24}$$

Expanding in series and neglecting higher-order terms, one has:

$$f' \simeq f \left(1 - \frac{v}{c}\right)$$

or (25)

$$f' - f = f_d = f \; v/c$$

More generally, assuming that the angle between the velocity vector v and the propagation path is δ, one has:

$$f_d = \frac{2 v \cos\delta}{c} \quad f = \frac{2 v \cos\delta}{\lambda} \tag{26}$$

where λ is the wavelength of the wave.

In practice, the scatter phenomena are accompanied by more-complex phase shifts depending upon the path-length spread due to beam widening and to time-varying of the distance. Assuming that the width of the received beam is θ (Fig. 9), the distance R varies between two limits R_o and R_m so that the corresponding phase of the returned wave is also varied between

$$\phi_o = \frac{4\pi R_o}{\lambda} \quad \text{and} \quad \phi_m = \frac{4\pi R_m}{\lambda} \tag{27}$$

In addition, the distance R_n varies in a small time interval with the law:

$$R_n(t) = R_n(t_o) - V (t-t_o) \cos\delta_n \tag{28}$$

Thus, if the transmitted wave is expressed as

$$E_T = \sum_{n=0}^{m} E_n \sin 2\pi f t \qquad (29)$$

the received wave assumes the expression

$$E_R = \sum_{0}^{m} G E_n \sin \left[2\pi f (t-t_o) - \frac{4\pi}{\lambda} R_n (t_o) - V(t-t_o) \cos \int_n \right] \qquad (30)$$

where G is a spread loss factor depending upon target-scattering properties. The latter equation shows that the reflected beam is characterized by a frequency spectrum rather than by a single frequency; in fact, writing Eq. 30 as follows:

$$E_R = \sum_{n=0}^{m} G E_n \sin \left[2\pi \left(f + \frac{2V \cos}{\lambda} n \right) (t-t_o) - \frac{4\pi}{\lambda} R_n (t_o) \right] \qquad (31)$$

one observes that a spread in frequency and in phase is obtained, depending upon the magnitude of the beamwidth θ. Reducing the latter by recourse to a laser beam is obviously beneficial.

There are two methods which may be used to apply laser doppler shift techniques; one consists in utilizing an unmodulated laser carrier and in measuring the shift of the optical frequency due to doppler effect, and the other one consists in utilizing a laser beam modulated with a microwave frequency and in measuring the doppler shift of the modulation rather than that of the carrier. The first technique requires recourse to optical heterodyning and takes advantage of the very high value of the optical frequency; for example, in the case of a HeNe laser, one has:

$$\lambda = 6328 \text{ Å}, \qquad f = 4.75 \times 10^{14} \text{ c/s}$$

The second technique requires recourse to microwave modulation and detection of laser carriers, but may utilize non-heterodyne-type detection; the basic frequency involved in the doppler effect is that of the modulating signal, which is, of course, many orders of magnitude lower than that of the laser carrier. Thus, the laser beam in this case may be useful as a narrow-beam carrier, since it permits the utilization of high-gain transmitting and receiving optical antennas. There appears to be considerable merit in the use of the second approach, mainly because it does not require heterodyne detection; however, difficulties are found in the design of efficient microwave modulators and detectors.

The first approach (i.e., unmodulated laser carrier and direct optical heterodyning) was investigated in our experimentation.

A block diagram of an optical laser radar is shown in Fig. 10; it consists of a CW laser, of an optical frequency translator, of an optical summing device such as an interferometer in which the reflected radiation is added in proper phase with the "local oscillator" component, and of a photodetector and radio-frequency receiver.

Assuming that the laser beam is very narrow, the signal returned from the wave surface of the sea will be deviated periodically following the continuous change of the orientation of the surface of incidence (Fig. 11); if the wave surface moves from Position A to Position B, the reflected laser beam is deviated from direction r_A to direction r_B. Therefore, the returned light enters the receiver aperture at different points and may even illuminate it only periodically for finite time intervals. This angular deviation complicates the heterodyne-detection phenomenon and must be taken into account; in the case of wide-beam return, the receiver aperture is continuously illuminated, but the angle of arrival may vary between values too large to satisfy the conditions for heterodyne detection, so that the detected signal is a pulse whose spectrum depends upon the amplitude and period of the sea-surface waves. A pulse is obtained when the laser beam has very small width, and the receiver aperture is illuminated periodically.

A rough analysis of this phenomenon can be developed assuming that the surface waves have a triangular form and that reflected laser beam is very narrow (Fig. 12); indicating with h the peak-to-peak amplitude and with λ the wavelength, the slope of the wave is given by the relation:

$$\tan \alpha = \frac{2h}{\lambda} \tag{32}$$

In order that a return is obtained in the direction of the incident beam, the latter must be directed within the angle characterized by the vertical and the normal-to-the-wave slope; the maximum angular deviation between reflected and incident beam is 2α, and the corresponding angular velocity of the reflected beam is:

$$\omega = 4\alpha/T$$

if the sea waves are stationary and have period T. The duration of the detected pulse is determined by the ratio between the angular aperture of the photodetector entrance pupil and the angular velocity of the reflected beam; i.e.,

$$\tau = D/R = DT/4\alpha R \tag{33}$$

where D is the diameter of the entrance pupil and R is the distance of the same from the point of incidence on the sea surface. In practice, the duration of the detected pulse depends also upon the width of the laser beam and upon the velocity of propagation of sea waves.

Recapitulating, although the transmitted beam is continuous, the reflected beam gives rise to a pulsed detected signal, whose characteristics of periodicity and duration depend upon the oscillatory motion and translational velocity of the sea waves, as well as on the width and relative orientation of incident and of scattered beam. Further modifications must be considered when the laser beam is made to scan a given area of the sea surface.

Following the concepts of design of the doppler laser shown in Fig. 10, the received pulse of duration τ and frequency $f_o + f_d$ is mixed with the local-oscillator signal, which has either frequency f_o or $f_o + f_t$; in the first case, one has a homodyne detector, and in the second case, one has a heterodyne detector, based on the use of a "frequency translation" of the laser carrier.

In general, it is desirable that the laser output be single mode and single frequency; single-mode operation (generally TEM_{00M}) possesses the highest possible degree of coherence, both spatial and temporal, and single-frequency operation provides unequivocal output of the heterodyne detector.

Single-mode operation may be obtained by proper design of the interferometric cavity[5] or by application of certain methods of frequency-locking and cancellation[6,7] ; single frequency and frequency stabilization means also have been investigated extensively[8].

Assuming that the relative radial velocity of the reflecting waves is v , the doppler frequency shift which appears at the output of the photodetector is:

$$f_d = 2v/\lambda \ ; \qquad (34)$$

for example, if $v = 1m/sec$ and $\lambda = 0.63\mu$, one has:

$$f_d = 3.17 \text{ mc/sec}$$

The receiver which follows the photodetector must be able to operate in a frequency range encompassing the expected doppler frequencies; if a frequency translation of the local oscillator is used, the receiver frequency range is reduced to $f_t - f_d$. Such frequency translation may be obtained by modulating the reflecting mirror of the Twyman-Green interferometer used to obtain superposition between reflected and local oscillator beams (Fig. 13); the bandwidth of the receiver must be sufficient to accept the energy of the returned pulse, which has duration τ ; i.e., $\Delta f = 1/\tau$. There follows that

the noise energy is determined by Δf. The receiver may be either a superheterodyne with a scanning local-oscillator frequency, or a broadband type with channelized input.

The operation of the optical heterodyne detector depends upon the coherent nature of the incident beams. Assuming that the signal and the local oscillator waves are cophasal over the entire surface of the photodetector and that their amplitudes and frequencies are respectively P_s, ω_s, P_r, ω_r, one finds that the input current resulting from mixing and optical detection is:

$$I_o = \frac{\eta q}{kT} \left[P_s + P_r + 2 \sqrt{P_s P_r} \cos (\omega_s - \omega_r)t \right] \qquad (35)$$

The ac component of this current has mean square value:

$$\overline{i_s^2} = 2 \left(\frac{\eta q}{h\nu} \right)^2 P_s P_r \qquad (36)$$

The mean square noise currents due to signal, local oscillator, dark current, radiation background, etc., are expressed as follows:

$$\overline{i_s^2} + \overline{i_r^2} + \overline{i_d^2} + \overline{i_b^2} = 2q \left(I_s + I_r + I_d + I_b \right) \Delta f \qquad (37)$$

where Δf is the receiver bandwidth, and I_s, I_r, I_d, I_b are the detected currents due respectively to signal, local oscillator, thermionic emission, background radiation.

The quantity η is the quantum efficiency of the photodetector; for S1 and for S20 surfaces, one has respectively $\eta = 1.5 \times 10^{-4}$ and 4×10^{-2}. The signal-to-noise ratio resulting from the consideration of the above relation is:

$$\frac{P_s}{N} = \frac{2 \left(\frac{\eta q}{h\nu} \right)^2 P_s P_r}{2q \left[I_s + I_r + I_d + I_b \right] \Delta f} \qquad (38)$$

If the local oscillator power is sufficiently large, the above relations may be simplified, letting:

$$I_s + I_d + I_b \ll I_r$$

$$I_r = \frac{\eta}{h\nu} P_r \qquad (39)$$

$$\frac{P_s}{N} = \frac{\eta P_s}{h\nu \Delta f}$$

This relation shows that the signal-to-noise ratio of coherent detectors is directly proportional to the quantum efficiency of the detector; if the local oscillator power is sufficiently large, the signal-to-noise ratio is independent of all noise sources except the photon noise $h\nu \Delta f$. The latter result is important and represents one of the major advantages of coherent versus noncoherent detectors.

However, in order to achieve operation of coherent detectors, it is necessary to assure very strict requirements of optical alignment. For example, if the target region illuminated by the laser beam has linear dimension of the order d and is at a distance R, then a necessary condition for the realization of spatial coherence is that the receiver aperture have diameter D_r where

$$D_r < \lambda R/d \qquad (40)$$

If the transmitter aperture diameter is D_t and the beam is collimated, the diameter of the spot size illuminated on the target is:

$$d = D_t + \lambda R/D_t \qquad (41)$$

Hence, the diameter of the receiver aperture must satisfy the condition:

$$D_r < \frac{D_t}{1 + (D_t^2/\lambda R)} \qquad (42)$$

At large ranges (i.e., when $R \gg D_t^2/\lambda$), one finds the simplified result:

$$D_r < D_t \qquad (43)$$

For example, if the transmitted laser beam has diameter 0.5 cm, the receiver

aperture diameter must be smaller than 0.5 cm . A practical system for optical heterodyne doppler measurements is shown in Fig. 14.

A study of the directional sensitivity of the receiver may be made, assuming that the transmitted and received waves are plane, with propagation vectors $\overline{k_1}$ and $\overline{k_2}$; if the detector surface is placed at $Z = 0$ (Fig. 15) the detected current possesses the following expression:

$$i(t) = \cos\left[(\omega_1 - \omega_2)t + \phi \right] \frac{\sin b \frac{D_r}{2}}{\frac{D_r}{2}} \qquad (44)$$

where

$$b = - k_1 \sin \theta_1 + k_2 \sin \theta_2 \qquad (45)$$

A plot of the amplitude of $i(t)$ versus $b\, D_r/2$ is shown in Fig. 16; it is seen that the amplitude becomes zero periodically in correspondence of the values $b\, D_r = 2n\pi$. If one assumes that $\theta_1 = 0$ (i.e., that the local oscillator beam is aligned so that its direction of propagation is along the normal-to-the-receiver surface), the first zero of the amplitude of $i(t)$ occurs when $k_2 \sin \theta_2 \cong k_2 \theta_2 = 2\pi$; i.e.,

$$\theta_2 \cong \lambda / D_r \qquad (46)$$

For instance, letting $\lambda = 0.6\mu$, $D_r = 0.5$ cm , one has $\theta_2 = 1.2 \times 10^{-4}$ rad. A typical plot of the angular sensitivity of the detector is given in Fig. 16; this shows that the heterodyne detection of two coherent plane wave beams is extremely sensitive to angular orientation.

In general, an heterodyne receiver is equivalent to an antenna; indicating with $A_r(\Omega)$ the effective aperture or capture cross-section for plane waves incident from direction Ω , the requirement of wavefront alignment between signal and local oscillator beams is translated into the condition

$$A_r \Omega_R \cong \lambda^2 \qquad (47)$$

While it is possible to trade off effective aperture and angular direction of arrival, it is not possible to modify the magnitude of the product which is very small. The condition (Eq. 47) imposes a severe limitation on the practical utilization of optical heterodyne detection for doppler laser radars; this is especially true when the distances R involved are larger

than 50 - 100 ft and when the turbulence of the atmospheric path and the randomness of the reflecting surfaces reduce the spatial coherence of the laser beam.

One additional limitation of the design is provided by the time-dependent characteristics of the received pulse and by the characteristics of the doppler signal. In fact, if the pulse duration is τ , the minimum doppler frequency which can be detected is $1/\tau$; this represents the speed resolution of the radar. For example, if $\tau = 1$ μsec and $\lambda = 0.63$, the minimum doppler frequency is $\sim$ 1 mc/s and the corresponding speed resolution is $\sim$ 0.315 m/sec = 1 ft/sec . Since the duration of the reflected received pulse signal is determined by the oscillatory and translational motion of the sea waves, the limit of resolution of the radar cannot be defined clearly.

4. EXPERIMENTAL INVESTIGATION OF THE DOPPLER FREQUENCY MEASUREMENTS BY OPTICAL HETERODYNE DETECTION

The experimental set-up built for the investigation of the doppler laser ASW radar is shown in Fig. 17. It consists of a HeNe laser operating at $\lambda = 0.6328\mu$; the optical cavity length is 1.20 m, and the mirrors are hemispherical (one flat and the other with radius 2 m). The diameter and divergence of the collimated beam are respectively 0.5 cm and 2×10^{-4} rad. The beam enters a Twyman-Green interferometer consisting of a beam splitter having 50% transmissivity, and is reflected back at the end of two arms by means of dielectric coated flat mirrors. The latter are mounted on piezoelectric crystals and are positioned by means of a 3-micrometers control system. A photomultiplier with S1 surface has been used as a detector; this was provided with suitable optical filter and iris.

Experiments were conducted with the interferometer arms of equal length (18 cm), and with one arm of length up to 5 m and the other of length 18 cm. In addition, reflections from a water tank were obtained.

Studies of heterodyne detection with equal arm length interferometer were made in the homodyne mode and in a heterodyne mode obtained by means of frequency translation of the "local oscillator" wave. In the first case, the "local oscillator" mirror was maintained at rest, and the "target" beam was made to vibrate sinusoidally, using the piezoelectric crystal control. The frequency of oscillation was varied in the range 0 - 1 mc. After fringes of interference were obtained on the surface of the photodetector in the static condition, clear mixing was seen to occur. The photomultiplier output examined with a spectrum analyzer indicated the presence of Fourier spectra consistent with the sinusoidal phase modulation realized with the vibration of the mirror.

From theory, one has that the analytical representation of the phase-modulated light wave is:

$$a = A_m \sin (\omega_o t + \phi_m \sin \omega_m t) \tag{48}$$

Expanding in a Fourier series, one has:

$$a = A_m \sin \omega_o t \left[J_o(\phi_m) + 2 J_2(\phi_m) \cos 2\omega_m t + \ldots \right. \\ \left. + A_m \cos \omega_o t \; 2 J_1(\phi_m) \cos \omega_m t + 2 J_3(\phi_m) \cos 3\omega_m t + \ldots \right] \tag{49}$$

i.e., using known trigonometric expansions:

$$
\begin{aligned}
a = {} & J_0(\phi_m) A_m \sin \omega_0 t \\
& + J_1(\phi_m) A_m \left[\sin(\omega_0 + \omega_m)t - \sin(\omega_0 - \omega_m)t \right] \\
& + J_2(\phi_m) A_m \left[\sin(\omega_0 + 2\omega_m)t + \sin(\omega_0 - 2\omega_m)t \right] \\
& + J_3(\phi_m) A_m \left| \sin(\omega_0 + 3\omega_m)t - \sin(\omega_0 - 3\omega_m)t \right| \\
& + \cdots\cdots\cdots
\end{aligned}
\qquad (50)
$$

The spectrum resulting from this type of modulation consists of sidebands at frequencies $\omega_0 \pm n\omega_m$, whose amplitudes depend upon the value of ϕ_m; an example corresponding to $\phi_m = 10$ is shown in Fig. 18.

Experiments with frequency translation of the local oscillator waves were conducted by modulating the mirror of the "local oscillator" arm with its piezoelectric mirror. The application of a sinusoidal modulation again results in a spectrum of the type shown above; in order to avoid spreading the energy on a large number of sidebands, it is desirable to use either a small value of ϕ_m or a suitable waveform of the modulation wave; for example, a ramp-like waveform would produce a single frequency, a sawtooth waveform would produce few spectral components, etc.

Experimental verifications of the above result are shown in Fig. 19, 20, and 21, where a modulating frequency of 100 kc was used for the "local oscillator" wave and a modulating frequency of 10 kc or 5 kc was used for the "target" wave. The spectrum analyzer was Panoramic Spectrum Analyzer Md SPA 3125, with a frequency range 0 - 23 mc/s. Figs. 19, 20, and 25 correspond to heterodyne mixing with 100 kc/s modulation of the local oscillator and 5 kc/s or 10 kc/s modulation of the "target" mirror. Note that, in Fig. 21, the magnitude of ϕ_m is selected so that the carrier amplitude of the sideband becomes zero; in Fig. 20, a single sideband at 100 kc, with the frequencies resulting from beating with it, is shown.

Mixing of the two incident waves was obtained also with greatly elongated arm of the "target" wave; in particular, a one-way distance of ~ 5 m was realized. At large distances, the alignment of the interferometer becomes more critical, and the fringe separation decreases with constant optical magnification.

The experimental set-up for reflection from water is seen in Fig. 22. In order to permit incidence at an angle for which a reflected beam direction coincidental with that of the transmitted beam may be obtained, the "depression" angle had to be of the order of 0 - 10°. This angle is shown in Fig. 22, where a practical set-up involving the use of an intermediate mirror

is indicated. Reflections from the surface of the water were obtained, and heterodyning was demonstrated easily in the absence of water waves.

Water waves of stationary and of traveling type were produced by means of a mechanical stirrer; frequencies of the order of 5 - 10 cycles were obtained. In addition, oscillations of much higher frequency, though of much smaller amplitude, were produced by means of piezoelectric transducer action. The heterodyne detection of the beams reflected from the water waves was not too satisfactory. The output of the multiplier appeared pulsed, as discussed in the previous section; the duration of these pulses was a function of the geometry of the system, but was too short to permit detection of the doppler signal.

5. DETECTION OF SIGNATURE BY OPTICAL FILTERING TECHNIQUES

Because of the limitations encountered in the application of doppler frequency measurements, a technique based on the detection of the optical signature by optical-filtering techniques was investigated. During the period covered by this report, the technique was investigated theoretically; equipment was built to provide a TV-like presentation of the sea-surface waves by illumination and scatter with a scanning laser beam. Experimental studies of matched optical filtering and of electronic filtering should be conducted in the following period.

The concepts of optical spatial filtering are based on the transform properties of lenses; ideally, a lens system transforms the light amplitude distribution in the front and back focal planes by means of a Fourier integral relationship. The basic observation of this property and its application to two-dimensional filtering of signal patterns was first introduced by Duffieux in France (1946) and was developed successively by Marechal[9], O'Neill[10], Gabor[11], and many others.

Consider the system of Fig. 23, which consists of an ideal lens of aperture D, illuminated by a monochromatic unpolarized wave having a cross-sectional complex modulation $E_o \tilde{f}(x,y)$, at the back focal plane; i.e.,

$$E_d(x, y, t) = E_o f_o(x, y) \exp j(\omega t + \phi(x,y)) \qquad (51)$$

At the front focal plane, the light distribution is expressed as follows:

$$E_s(x' y') = E_o e^{j\omega t} \iint_P f_o(x,y) \exp j(\phi(x,y) + \omega_x x + \omega_y y)\, dx\, dy \qquad (52)$$

where $\omega_x = 2\pi x'/\lambda F$, $\omega_y = 2\pi y'/\lambda F$ are called "radian spatial frequencies," and x', y' are coordinates in the front focal plane. The above integral expression (52) is extended over the pupil P of the system and, except for the latter limitation, represents the Fourier transform of the function $\tilde{f}(x,y) = f_o(x,y) e^{j\phi}$. Thus, normalizing the integral (52), one has:

$$\tilde{E}_s'(x',y') = \iint_P f_o(x,y) \exp j(\phi(x,y) + \omega_x x + \omega_y y)\, dx\, dy \qquad (53)$$

This constitutes a two-dimensional display which may be retransformed into the signal by means of a second lens as shown in Fig. 24; at plane P_o, a suitable spatial filtering function may be introduced in order to enhance the signal-to-noise ratio for a desired pattern. For example, assume that a

transparency $\bar{T}(x',y')$ is placed at plane P_2, thus producing the product $\bar{E}_s'(x', y')\,\bar{T}(x', y')$; the image produced at plane P_3 is the convolution of $\bar{f}(x, y)$ and $\bar{t}(x, y)$; i.e.,

$$\bar{f}(x, y) * \bar{t}(x, y) = \iint f(\xi, \eta)\; t(x-\xi, y-\eta)\; d\xi\, d\eta \qquad (54)$$

It is therefore possible to modify the spatial frequency content of a light signal distribution in a manner analogous to that of electrical filters which modify the temporal frequency content of electrical signals. In particular, using this technique, one can utilize optimum smoothing filters if a contour obscured by other detail is to be detected in its original form, or matched filters if recognition of the pattern is sufficient; in the latter case, the filter acts to suppress the noise and to concentrate the energy of the signal into a small area.

To illustrate the operation of a matched filter, consider again the case of a signal $\bar{f}(x, y)$ having Fourier transform $\bar{E}_s(x', y')$; and assume that the signal is superimposed on a noise background $n(x, y)$. The matched filter is a transparency having the following transmittance function:

$$\bar{T}(x', y') = K\,\bar{E}_s^*(x', y') \qquad (55)$$

At the focal plane P_2, the signal consists of a wavefront whose contour is characterized by a phase distribution $\phi(x' y')$. By application of the matched filter (55), the phase is compensated for, resulting in a constant value; i.e., in a plane wavefront. This wave is then focussed by lens L_2 into a point in plane P_3, having large intensity and located at the coordinates corresponding to the original position of the signal in plane P_1. The matched filter also operates on the amplitude of the Fourier transform of the signal, attenuating the noise where the signal is weak and thus enhancing the resultant signal-to-noise ratio.

In order to take advantage of the signal-processing properties of optical systems, it is necessary to use monochromatic, coherent light illumination. The realization of complex matched filters poses a difficulty because such filters are generally obtained with photographic film transparencies in which the transmittance can only be positive or zero, and the phase cannot be controlled simply. (Attempts to control the phase by variation of the thickness have proven awkward.) A much simpler design of complex filters has been developed recently[12, 13].

Assume that a transparency with the complex transmittance function

$$\bar{T}(x', y') = \left| T(x', y') \right| e^{j\phi(x', y')} \qquad (56)$$

must be built. One makes a mask having the real transmittance function

$$T_\beta + \left| T(x', y') \right| \cos \left(x_o x' + \phi(s', y') \right) \qquad (57)$$

This function consists of a constant bias term T_β (which is necessary because the transparency must remain positive everywhere); and of two complex terms, respectively

$$\frac{1}{2} \left| T(x', y') \right| \exp j \left(x_o x' + \phi(x', y') \right) = \frac{1}{2} \bar{T}(x', y') \epsilon^{j x_o x'}$$

$$\frac{1}{2} \left| T(x', y') \right| \exp -j \left(x_o x' + \phi(x', y') \right) = \frac{1}{2} \bar{T}^*(x', y') \epsilon^{-j x_o x'} \qquad (58)$$

Placing the above transparency at focal plane P_2, one obtains the convolution of the signal distribution function $\bar{f}(x, y)$ with each of the terms of (57) ; i.e.,

$$T_\beta \bar{f}(x, y) + \bar{t}(x - x_o, y)^* \bar{f}(x - x_o, y) + \bar{t}^*(-x_o + x, -y)^* \cdot \bar{f}(-x + x_o, -y) \qquad (59)$$

In order to illustrate the derivation of the results of Equ. 59, we recall that multiplication of a real function by an exponential corresponds to a translation of variable in the complex frequency domain; i.e., if $\bar{F}(x')$ is the Fourier transform of $\bar{f}(x)$, then $\bar{F}(x' - \alpha)$ is the Fourier transform of $\bar{f}(x) \epsilon^{j\alpha x}$; similarly, $\bar{F}^*(x' + \alpha)$ is the Fourier transform of $\bar{f}^*(x) \cdot \epsilon^{-j\alpha x}$.

Thus, the derivation of Eq. 59 by convolution of the signal function with each term of the transmittance (57) is clear; the first term of Eq. 59 is proportional to the original signal, attenuated by the constant factor T_β , the second term is the desired matched filter output, displaced by a distance x_o from the signal of the first term, and the third term is still another filter output obtained with a filter function which is the conjugate of that of the second term, displaced by a distance $-x_o$. The displacement x_o is purposely introduced in order to avoid overlapping of the three terms of Eq. 59 and to permit their separation.

Recapitulating, we have shown that a transparency having a real transmittance function type (Eq. 57) may be used to provide a complex matched filter operation. The preparation of the transparency (Eq. 57) may be made by various methods; an elegant approach (Ref.12) is one based on the use of a modified Mach-Zender interferometer (Fig. 25). The function $\bar{t}(x,y)$, whose Fourier transform is Equ. 56, is placed in one beam of the interferometer, so that the corresponding Fourier transform produced by lens L_1 is displayed at its back focal plane outside the interferometer. Indicating with $\bar{r}(x,y)$ the light distribution from a reference beam, whose Fourier transform is $\bar{R}(x',y') = R_o \exp j\,(x_o\,x' + y_o\,y')$, one has the following resultant light distribution at the output plane P_2 :

$$\bar{R}(x',y') + \bar{T}(x',y') = r_o\, \epsilon^{j(x_o\,x' + y_o\,y')} + \left|T(x',y')\right| \epsilon^{j\phi(x',y')} \tag{60}$$

At plane P_2, a photographic plate with suitable exposure slope is placed; this gives a transparency proportional to the energy output; i.e.,

$$G\,(x',y') = \left|\, R(x',y') + T(x',y') \,\right|^2 = \left|\, R(x'y') \,\right|^2 + \left|T(x',y')\right|^2 + \\ + 2\left|\, R(x',y'')\right| \left|\, T(x',y') \,\right| \cos\,(x_o\,x' + y_o\,y' + \phi(x',y')\,) \tag{61}$$

Substituting the expression of $\bar{R}(x',y')$, one finds:

$$G(x',y') = R_o^{\,2} + \left|\, \bar{T}(x',y') \,\right|^2 + 2R_o \left|\, T(x',y') \right| \cos\,(x_o\,x' + \\ + y_o\,y' + \phi(x',y')\,) \tag{62}$$

Thus, the required transfer function type (Eq. 57) is obtained.

6. DETECTION OF SIGNATURE BY ELECTRONIC FILTERING PROCESSES OF PATTERN RECOGNITION

When viewing a picture, the human eye is found to be more sensitive to the detection of edges (i.e., of abrupt rather than of continuous charges of brightness). This property has been utilized in the study of television bandwidth reduction systems[14]. With reference to Fig. 26, the video signal obtained by scanning a picture is split into two paths--one routed through a low-pass filter of frequency response $L(j\omega)$, and the other one routed through a differentiator. The former portion is limited to the information corresponding to the slow varying signal intensity, while the latter provides a large output in correspondence of abrupt signal variations, by forming the derivative $\frac{ds}{dx}$, where x is the scanning variable proportional to time. Thus, the latter channel contains predominantly edge information. At the receiving end of the TV transmission system, the edge-information signal is passed through a filter whose transfer function is:

$$H(j\omega) = \frac{1 - L(j\omega)}{j\omega} \tag{63}$$

The output of the latter is added to the slowly varying portion of the information and reproduces the original picture.

A generalization of the method of edge detection has been proposed recently[15] with application to two-dimension processing. The method is illustrated in Fig. 27 and utilizes a gradient operator, consisting of a pair of two-dimensional filters H_1 and H_2, which synthesize the high-frequency part of the picture. Using appropriate transfer functions $H_1(ju, jv)$ and $H_2(ju, jv)$ at the receiving end, and recombining the outputs as in the case of Fig. 26, one reconstitutes the original picture.

These methods have the advantage of requiring a smaller bandwidth than that of conventional TV transmissions; thus, bandwidth reductions as high as 7:1 and 15:1 have been demonstrated. Examples of application are shown in Fig. 28[16].

While the above-described method was developed predominantly for the purpose of bandwidth reduction, it can be readily modified for the recognition of V-shaped patterns such as are of interest in the detection of optical signatures of submarines.

7. EXPERIMENTAL WORK IN CONNECTION WITH THE INVESTIGATION OF OPTICAL AND ELECTRONIC FILTER TECHNIQUES OF PATTERN RECOGNITION

For the study of optical matched filter and electronic edge-enhancement filter techniques, an experimental system consisting of a laser illuminator, beam scanner, receiver-collector and photodetector, electronic rate counter, staircase cathode-ray tube, display signal generator, memory-type oscilloscope display has been built.

The block diagram of the laboratory model is shown in Fig. 29. It consists of a CW visible laser (HeNe, $\lambda = 6328\text{Å}$, $P_{out} \cong 5$ mW) whose collimated output is scanned mechanically by means of a pair of reflecting prisms with axes perpendicular to each other (Fig. 30); the prisms are driven with step-type motors which are actuated by pulse trains. The repetition rate of each pulse train may be varied at present up to values of 45 pulses/sec for the faster unit (line scanner), and the repetition rates of the two pulse trains are always maintained with a constant ratio 15:1. In the present unit, each pulse produces a rotation of 3° of the axis of the prism; thus, after 15 pulses, a total rotation of 45° is obtained, and a new face of the prism is presented to the laser beam. While one prism rotates 45°, the other one rotates 3°, and so on. Thus, one prism acts as a line-stepper, and the other one as a frame-stepper. Increasing the number of faces of the prisms and reducing the rotation per step, any angle of scan in the vertical and in the horizontal direction can be obtained.

The pulse trains are generated by a clock consisting respectively of an astable silicon-controlled rectifier circuit, oscillating at the faster rate, and by a monostable silicon-controlled rectifier circuit, which is triggered periodically by one of the pulses of the first train, maintaining a fixed ratio of 15:1 between the two trains.

The clock generator is also utilized to produce a precision stair-case voltage for the synchronous control of the two-dimensional scanning of the readout scope. The latter circuit, which was developed along principles believed to be novel, is illustrated in Fig. 31. Two stair-case waveforms are obtained respectively for the horizontal and for the vertical deflection control. Each waveform consists of 15 levels or steps, and is obtained by recourse to a nonlinear network consisting of diode-resistance circuits in which the biases of a number of diodes are progressively changed from "off" to "on", or vice versa, by means of pulse-controlled SCR pulse generators. With reference to the schematic of Fig. 31, a dc voltage is applied across the divider from A to B and from A' to B'. The divider is tapped at 15 points equally spaced in resistance values.

Initially, when power is first turned on, the voltage at Points 1 through 15 are at zero potential, because the SCR's are not conducting. This is true for both horizontal and vertical circuits. Diodes D1 through D15, and D1' through D15', are forward-biased, and therefore Diodes d1 through d15, and d1' through d15', are reverse-biased; as a result, the output is 0 volts for both horizontal and vertical outputs.

The voltages at the divider taps will appear one at a time across the load, respectively H and V terminals, when the corresponding diode of the D1-to-D15 group or D1'-to-D15' group becomes reverse-biased. Since the voltages at the control points of these diodes are applied sequentially, the output becomes a stair-case function.

A ring-counter circuit is used to apply pulses sequentially to the control terminals 1 through 15. The design of this circuit is based on the use of cathode coupling; it will be noted that, with this type of coupling, the "on" SCR does not "turn off" until the next SCR is "on"; this feature is essential in order to prevent occurrence of "drop" in the output stair-case voltage waveform.

The clock switches the ring counter from one stage to another, and consequently switches the output to the next step. The clock pulses have no effect on the ring counter until both "set" switches are momentarily closed.

Photographs of the stair-case voltage and of the corresponding two-dimensional scope display are shown in Figs. 32 and 33 respectively.

As seen from the block diagram of Fig. 29, the received laser signal is first applied to an optical signal-processing unit and, subsequently, is detected with a photomultiplier (surface S1 or S20). The output of the latter is proportional to the reflected light signal and may be applied directly (Switch S closed) to the z-axis of the display-scope, thus providing an optical representation of the reflection from the sea surface. An electronic picture-processing unit is expected to be interposed between photomultiplier and display scope to provide pattern enhancement by edge detection. In the present set-up, the optical processing unit and the electronic processing unit have not yet been developed. This mode of operation of the Laser Detection system results in a television-type picture presentation and may be associated with a fast scanning of the sea-surface area under observation. Wake patterns are extracted from the noise background represented by the wind-generated waves and are viewed directly.

An additional mode of operation of the Laser Detection system is shown in Fig. 31 and is obtained by opening Switch S; in this case, a Rate Counter unit is interposed between photomultiplier output and electronic signal-processing unit, to provide a signal proportional to the rate of oscillation of the waves rather than to the size of their reflecting facet. The Rate Counter has already been built; it consists of a pulse-shaping circuit, in which the received pulses are converted into rectangular pulses of uniform amplitude and duration, and of an integrator circuit whose output voltage is proportional to the rate of oscillation of the waves. In this mode of operation, a pattern different from the "wake" is obtained on the scope, namely, a pattern representing loci of constant oscillation rate; since the mean frequency of sea waves is of the order of 10-20 per sec for capillary waves and of the order of 1-2 per sec for gravity waves, the scanning speed of the read-out laser beam must be adapted accordingly, with a value lower than for wake pick-up.

Photographs of the equipment built and described above are shown in Fig. 34 and Fig. 35; these include the Laser, the Scanner and a small water tank, and the Rack-mounted Receiving unit and oscilloscope.

In its present form, the Optical Signature Detection system provides a 15 x 15 matrix-type display which is intensity-modulated as a function of the laser reflection from the water surface. An example of pattern taken with an optical collector of small aperture is given in Fig. 36; only a few illuminated spots appear on the scope because, due to the absence of diffusion at the reflection from the surface of the water, the returned beam remains collimated and misses the optical collector at a number of points.

In order to apply the techniques of optical matched filtering, a suitable transparency must be built; as previously indicated, the aim of the filtering process is the optimization of the peak signal energy with respect to mean-square noise energy. If one indicates with $\bar{f}(x,y)$ the signal and with $n(x,y)$ the noise, and assumes that the latter is a homogeneous isotropic random process with spectral density $N(x',y')$, the solution of the problem is obtained by recourse to a filter having the following transmittance function[12]:

$$H(x'\ y') = k \frac{\bar{F}^*(x',y')}{N(x',y')} \tag{64}$$

where $F^*(x'y')$ is the complex conjugate of the signal spectrum and k is a constant. One realizes the above transfer function by means of two transparencies placed in contact with each other; the first transparency represents $F^*(x',y')$ and is made by recourse to the Mach-Zender interferometer, previously illustrated (Fig. 25). The second transparency represents $1/N(x',y')$ and is made from a photograph of the distribution $n(x,y)$, first by producing the Fourier transform $N(x',y')$ and then recording it on a suitable film. If D is the density of the film, the specular amplitude transmission is $T = \exp(-D/2)$. The relationship between density D and exposure E of the film is given by the following relationship:

$$D = \gamma (\log E - \log E_0) \tag{65}$$

where γ and E_0 are characteristics of the film and of its development process; therefore, one has:

$$T = C E^{-\gamma/2} \tag{66}$$

Making E proportional to $N(x',y')$ and $\gamma = 2$, the specular transmission T is proportional to $1/N(x',y')$.

The transparency proportional to $F^*(x',y')$ may be made taking as reference photographs of typical wake patterns in the absence of noise.

It is of interest to recall some results of pattern recognition reported in the literature[12]. Several geometric patterns are shown in Fig. 37; those with symmetry (such as the rectangles) have a real Fourier transform, while those without symmetry (such as the letter L) have a complex Fourier transform. The complex Fourier transform of the letter L is shown in Fig. 38; this was taken by means of a Mach-Zender interferometer and consists of various components--i.e., a center component corresponding to the first two terms of Eq. 61, and two side components corresponding to the two exponential components of the last term of Eq. 61 (as shown in connection with Eq's. 57 and 58.) Finally, the cross-correlation of the L mask with the input function is shown in Fig. 39 and appears as a brilliant symmetrical signal[17].

8. CONCLUSIONS

The problem of the detection of the optical signature of submarines may be approached successfully by means of laser techniques. The general method discussed in this report is based on the use of an unmodulated laser beam which illuminates the sea surface from the air and is scattered with variable intensity, optical frequency, angular direction, polarization, depending upon the state of the sea surface. In particular, the optical frequency variations depend on the relative velocity of the sea waves and may be measured by means of doppler techniques; unfortunately, the application of these is extremely difficult and impractical at optical frequency, due to the fact that the heterodyne detector acts as an antenna whose aperture A_R and angle of arrival of received rays Ω_R must satisfy the condition $A_R \Omega_R \cong \lambda^2$, where λ is the optical wavelength.

A much more practical method of detection of the optical signature is one based on the detection of the modulation of the angular direction of scatter of the laser beam, which varies periodically with the oscillations of the sea waves, and on the realization of a TV-like representation of the sea surface, with the utilization of optical matched filters for the enhancement of the signal-to-noise ratio.

REFERENCES

1 A. H. Schooley - "The Fine Structure of Water Waves"; U.S. Nav.Res. Lab (1960).

2 A. H. Schooley - "Profiles of Wind-Created Water Waves in the Capillary Gravity Transition Region"; J. MARINE RES. Vol. 15, N.2, (1958), p. 100.

3 G. C. Cropper - "Exact Solution for Progressive Capillary Waves"; J. FLUID MECH. Vol. 2 (1957), p. 532.

4 J. J. Stokes - Water Waves; Interscience Publ. (1957), p. 225.

5 G.D.Boyd and H. Kogelnik - "Generalized Confocal Resonator Theory"; BSTJ, Vol. 41 (July 1962), pp. 1357 - 1369.

6 S. E. Harris - "Control and Stabilization of Laser Oscillators by Internal Time-Varying Perturbation"; PROC. IEEE, Vol. 54 (Oct. 1966), pp. 1401 - 1413.

7 P. N. Smith - "Stabilized Single-Frequency Output from a Long Laser Cavity"; IEEE J. QUANTUM ELECTR. Vol. QE1 (Nov. 1965), pp. 343 - 348.

8 A. D. White - "Frequency Stabilization of Gas Lasers"; IEEE J. QUANTUM ELECTR. Vol. QE1 (Nov. 1965), pp. 349 - 357.

9 A. Maréchal - Optical Processing of Information; edited by D.K.Pollack et al, Spartan Books, Baltimore (1963).

10 E. O'Neill - "Spatial Filtering in Optics"; IRE TRANS. INFO. THEORY, (June 1956), p. 55.

11 D. Gabor - NATURE, 161 (1948) p. 777; PROC. PHYS. SOC. (London), B64 (1951), p. 449.

12 A. VanderLugt - "Signal Detection by Complex Spatial Filtering"; IEEE TRANS. INFO. THEORY, IT-10, Vol. 2 (1964), p. 139.

13 E. N. Leith, A. Kozma, J. Upatnicks - Coherent Optical Systems for Data Processing, Spatial Filtering, and Wavefront Reconstruction · Optical and Electrooptical Information Processing; MIT Press (1965), p. 143.

14 W. F. Schreiber, C. F. Knapp - "TV Bandwidth Reduction by Digital Coding" ; IRE NAT. CONV. REC., Part 4 (1958), p. 88.

15 W. F. Schreiber - "The Mathematical Foundation of the Synthetic Light System" - Quarterly Progress Rept. of Res. Labs. of Electronics, MIT No. 68 (1963), p. 140.

References (Cont'd)

16 T. S. Huang, O. J. Tretiak - Research in Picture Processing Optical and Electrooptical Information Processing; MIT Press (1965), p. 45.

17 Examples of Matched Filters for Photographs of Wakes are shown in G.L.Hall - "The Application of Lasers to Spatial Frequency Filtering for the Analysis of Wakes (U)" - Classified Report, PROC. SECOND LASER TECHN. CONF. (1965), Chicago.

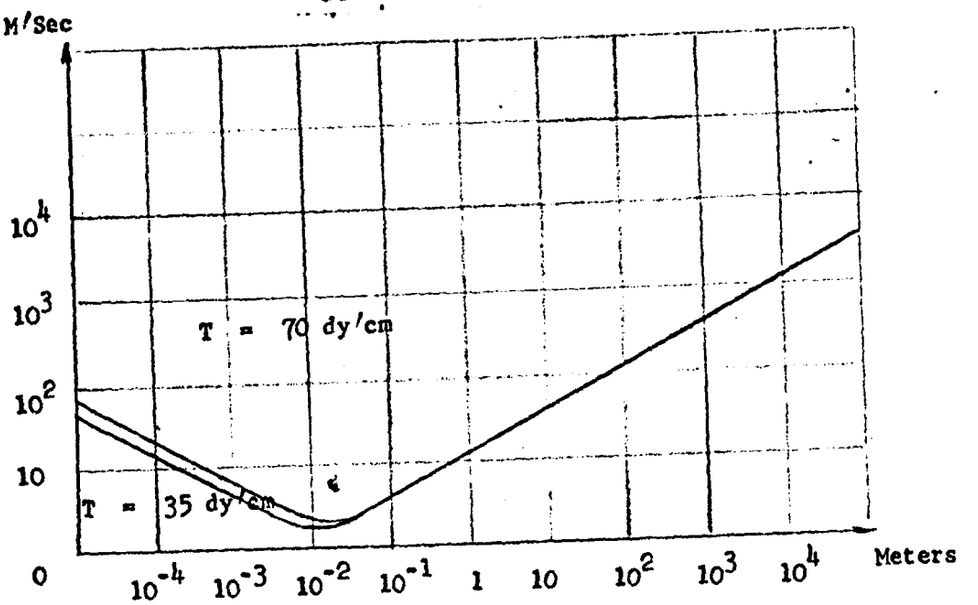

FIG. 1 - WAVELENGTH (Ref. 1)

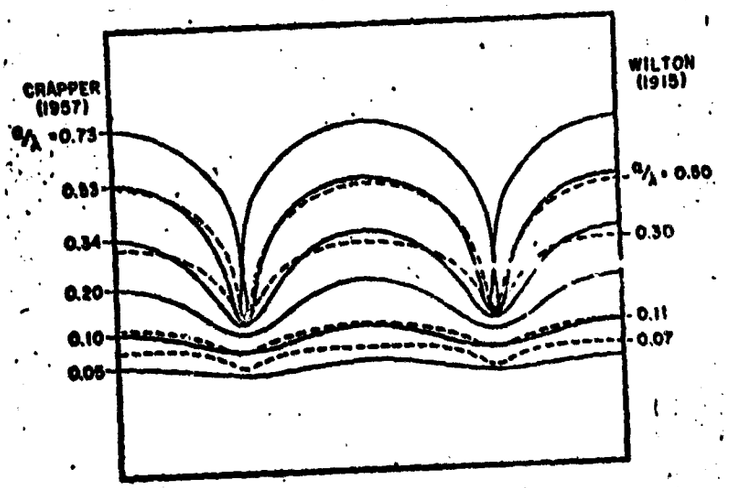

FIG. 2 - PROFILES OF CAPILLARY WAVES (Ref. 1,2,3)

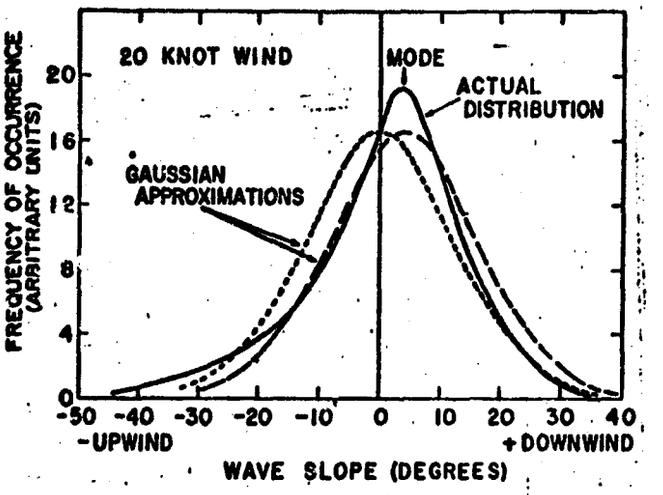

FIG. 3 - STATISTICAL DISTRIBUTION OF WAVE SLOPES (Ref. 1)

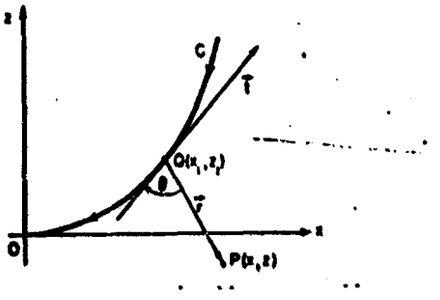

FIG. 4 - NOTATIONS FOR ANALYSIS OF WAKE

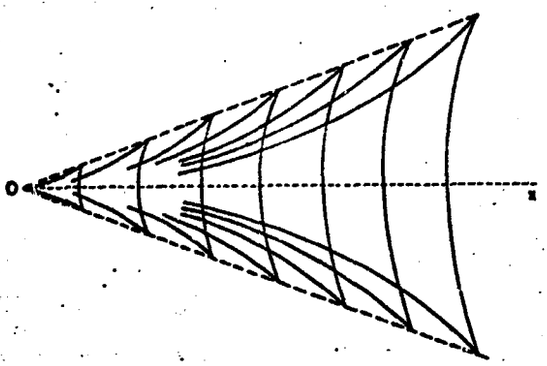

FIG. 5 - WAKE WAVES FOR STRAIGHT COURSE AT CONSTANT SPEED (Ref. 4)

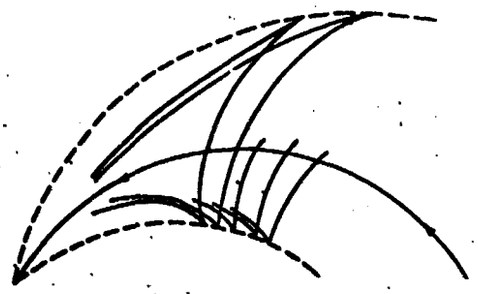

FIG. 6 - WAKE WAVES FOR CIRCULAR COURSE AT CONSTANT SPEED (Ref. 4)

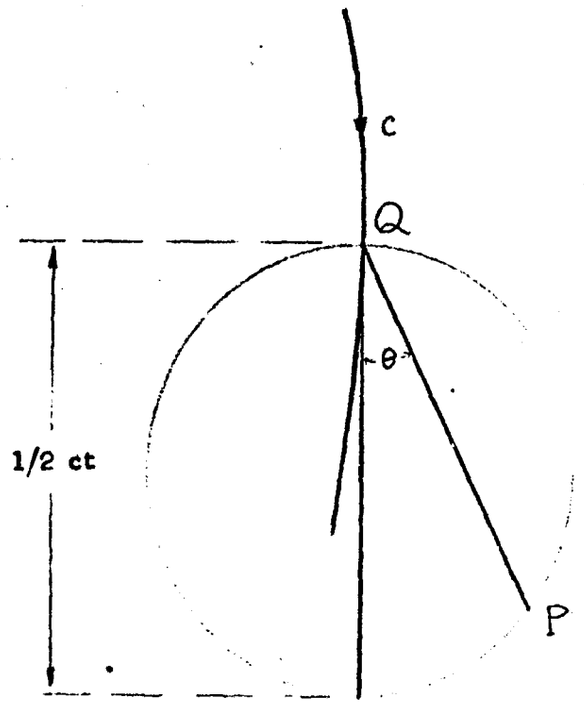

FIG. 7a - GEOMETRICAL CONSTRUCTION OF INFLUENCE POINTS

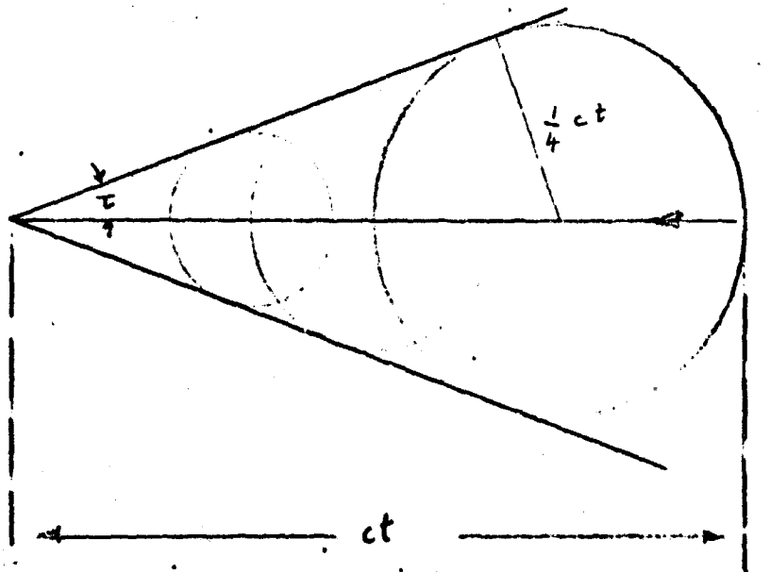

FIG. 7b - GEOMETRICAL CONSTRUCTION OF WAKE BOUNDARY FOR STRAIGHT COURSE

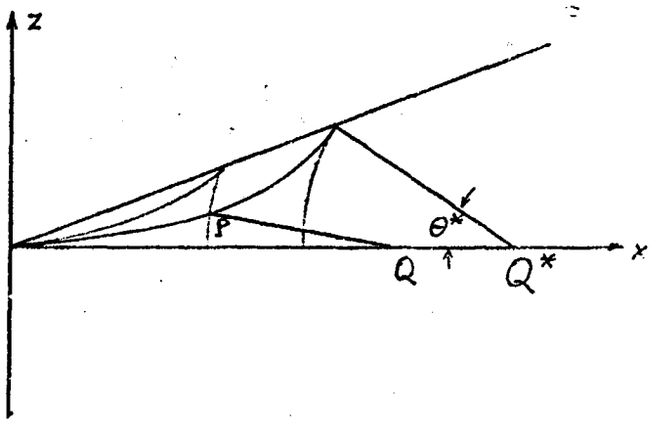

FIG. 8 - CONSTANT-PHASE CURVES

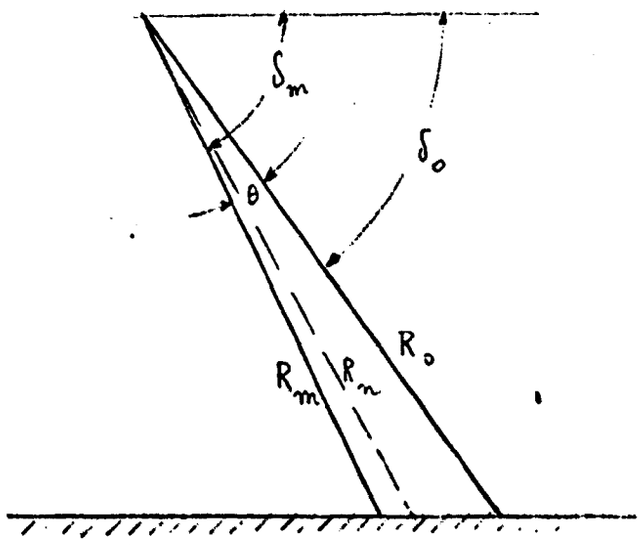

FIG. 9 - EFFECT OF BEAM WIDTH ON DOPPLER FREQUENCY VALUE

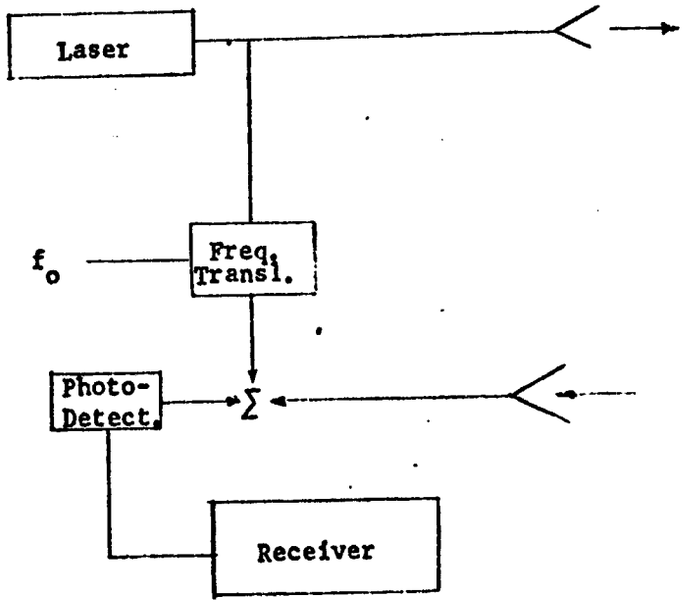

FIG. 10 - BLOCK DIAGRAM OF OPTICAL LASER RADAR

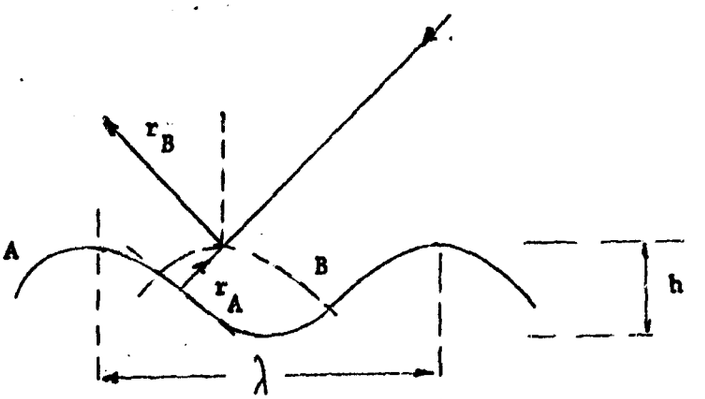

FIG. 11 - ANGULAR DEVIATION OF REFLECTED RAY

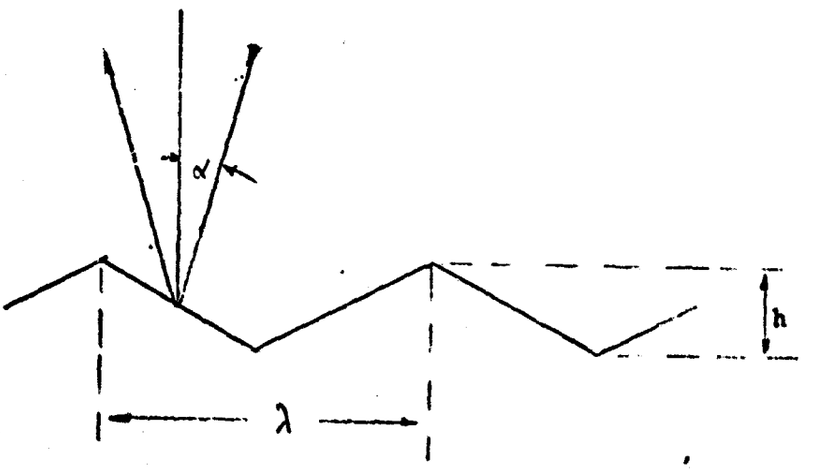

FIG. 12 - ANALYSIS OF ANGULAR DEVIATION OF REFLECTED RAY

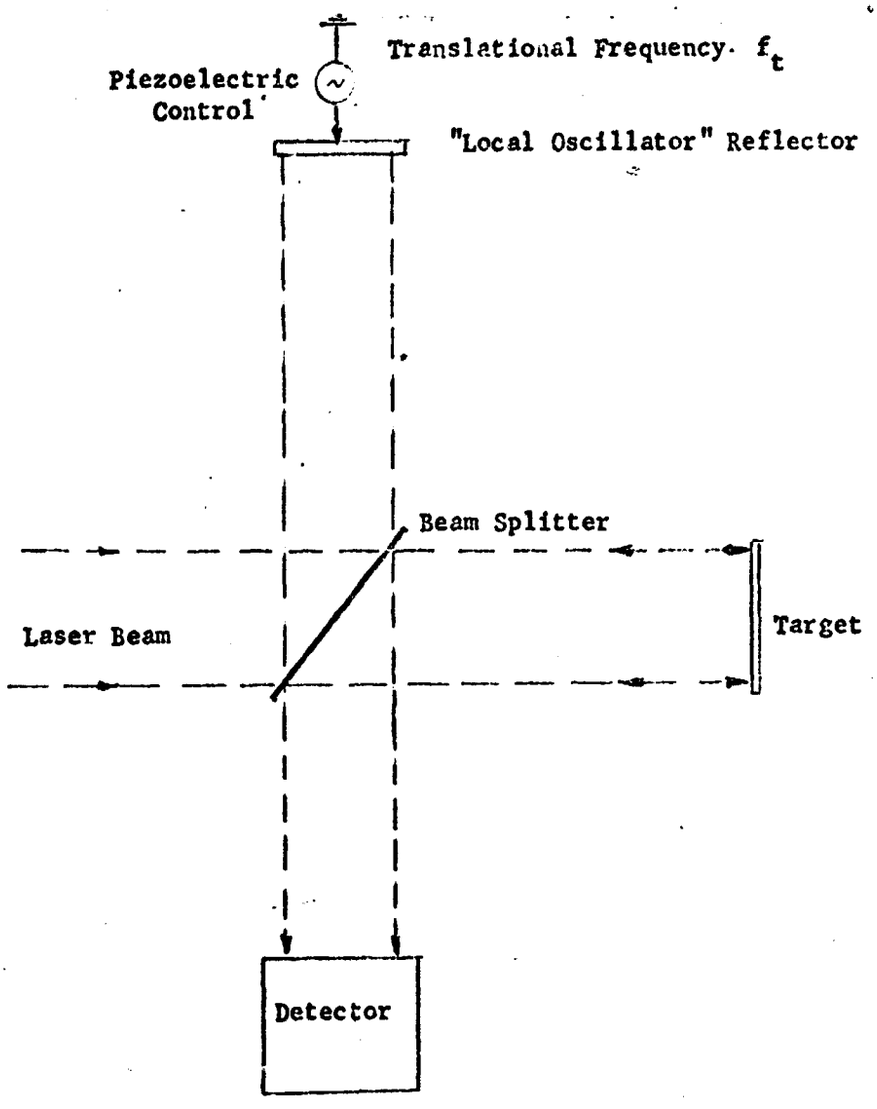

FIG. 13 - SCHEMATIC OF HETERODYNE SYSTEM WITH FREQUENCY TRANSLATION

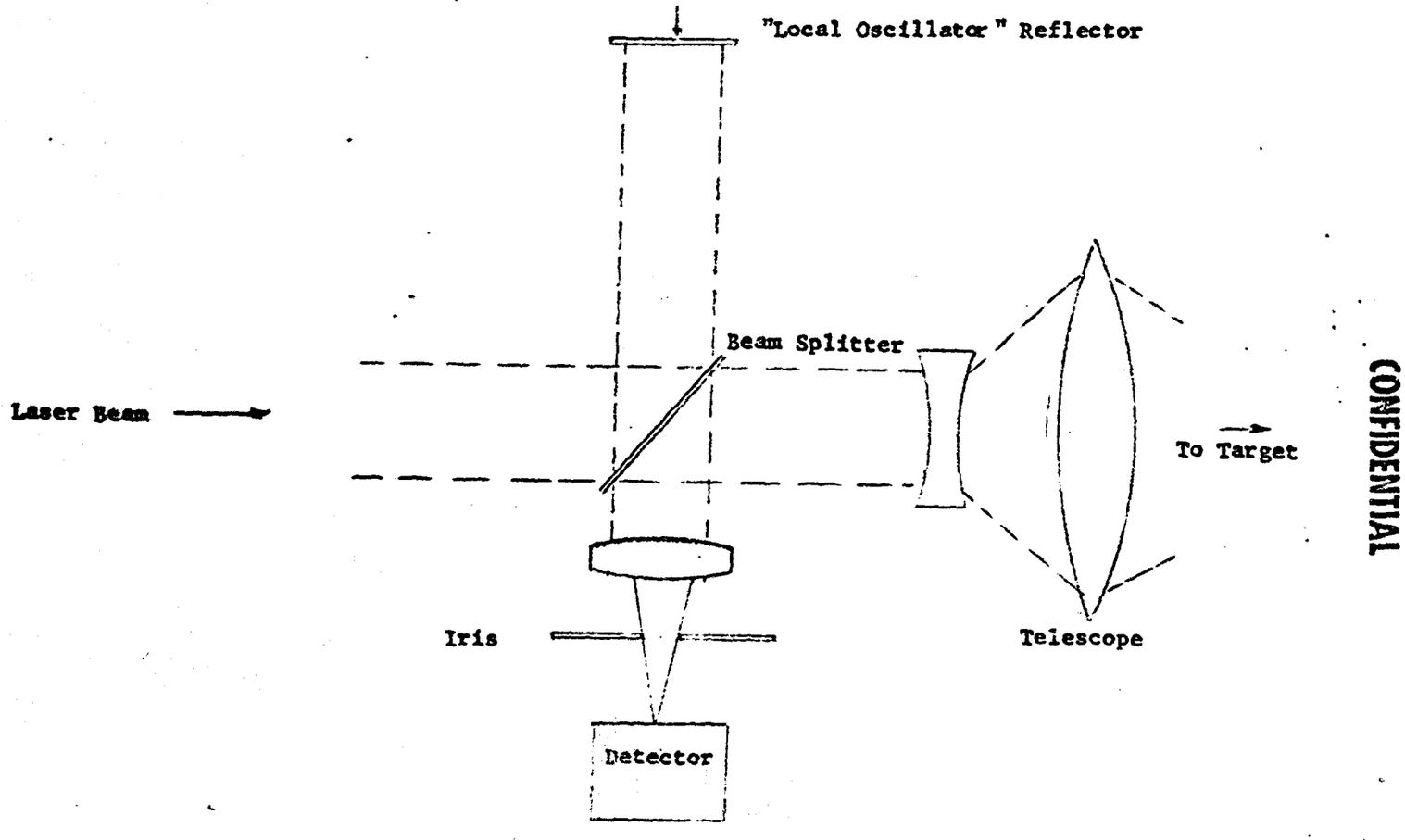

FIG. 14 - EXAMPLE OF PRACTICAL HOMODYNE OR HETERODYNE SYSTEM

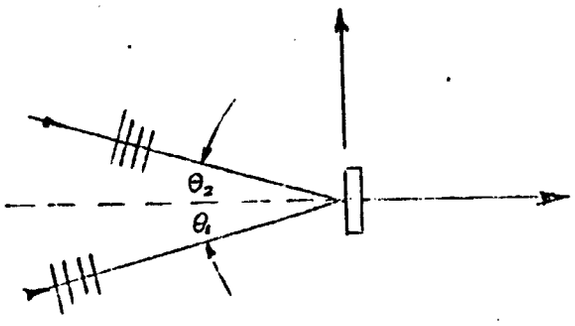

FIG. 15 - OPTICAL MIXING AT PHOTODETECTOR SURFACE

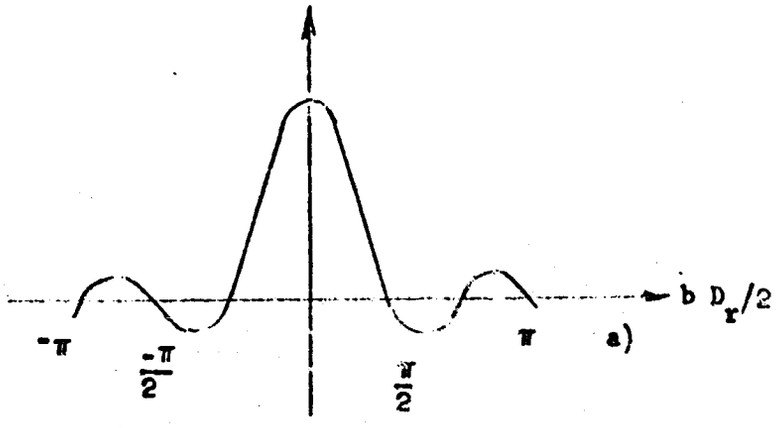

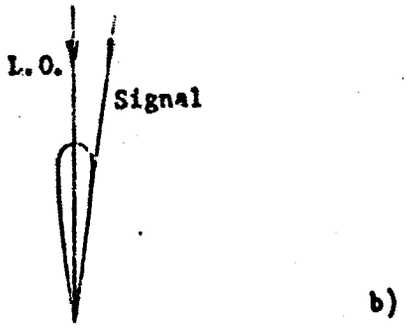

FIG. 16 - a) PLOT OF AMPLITUDE OF DETECTED SIGNAL VERSUS $bD_r/2$

b) TYPICAL ANGULAR SENSITIVITY OF HETERODYNE DETECTION

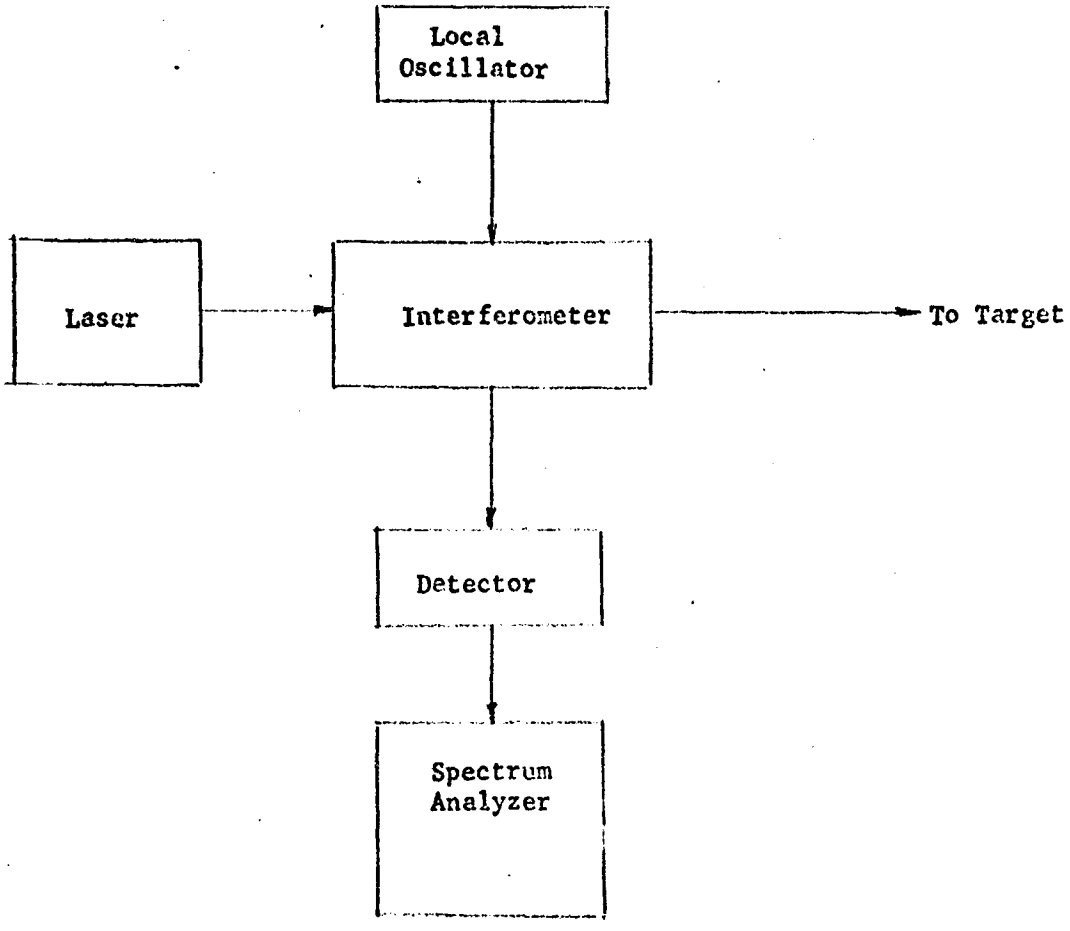

FIG. 17 - EXPERIMENTAL DOPPLER LASER RADAR SYSTEM

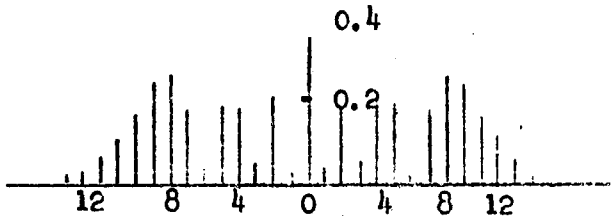

FIG. 18 - TYPICAL FM SPECTRUM CORRESPONDING TO $\phi_m = 10$

FIG. 19 - MODULATION OF LOCAL OSCILLATOR AT 100 kc, AND MODULATION OF EACH SIDEBAND COMPONENT AT 10 kc.

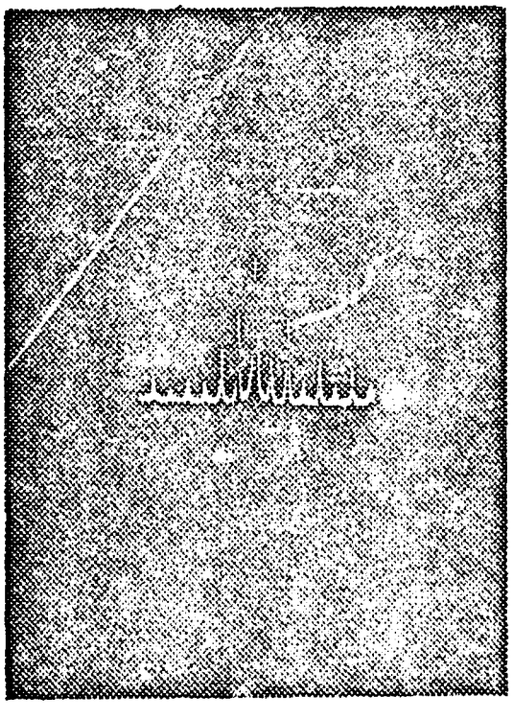

FIG. 20 - ENLARGED VIEW OF THE SPECTRUM SURROUNDING ONE OF THE SIDEBAND COMPONENTS OF Fig. 19.

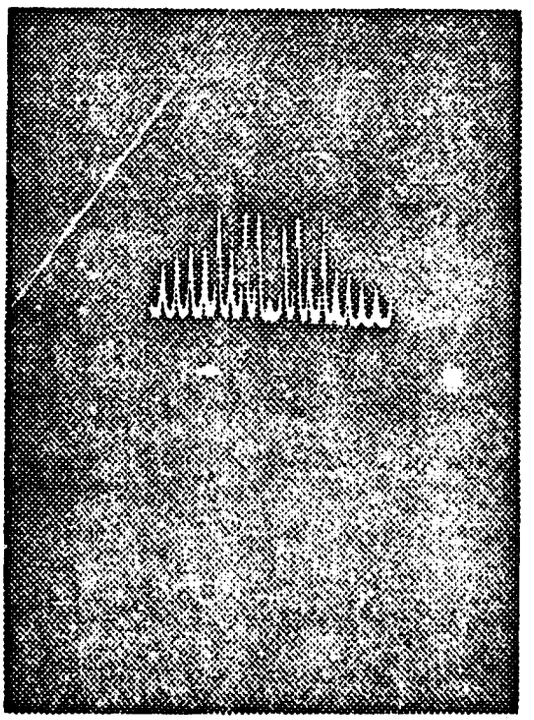

FIG. 21 - SPECTRUM RESULTING FROM MODULATION OF THE LOCAL OSCILLATOR AT 100 kc AND MODULATION OF THE TARGET AT 5 kc.

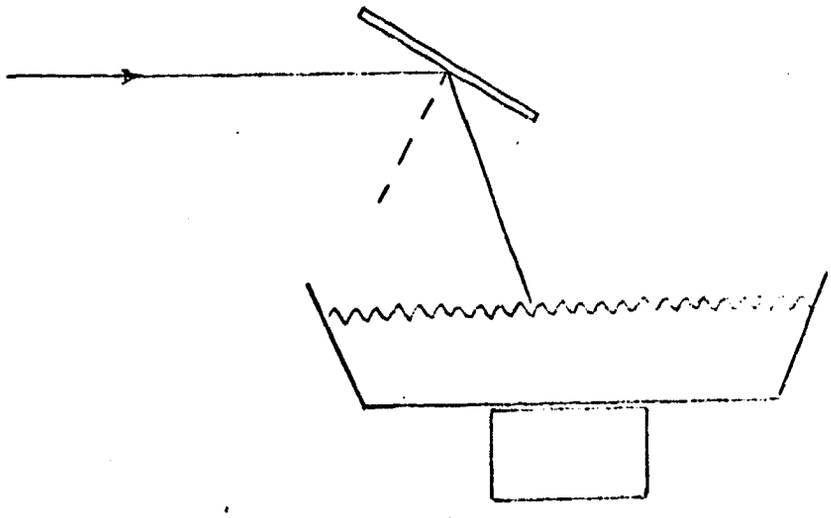

FIG. 22 - EXPERIMENTAL SET-UP FOR STUDY OF REFLECTIONS FROM WATER SURFACE

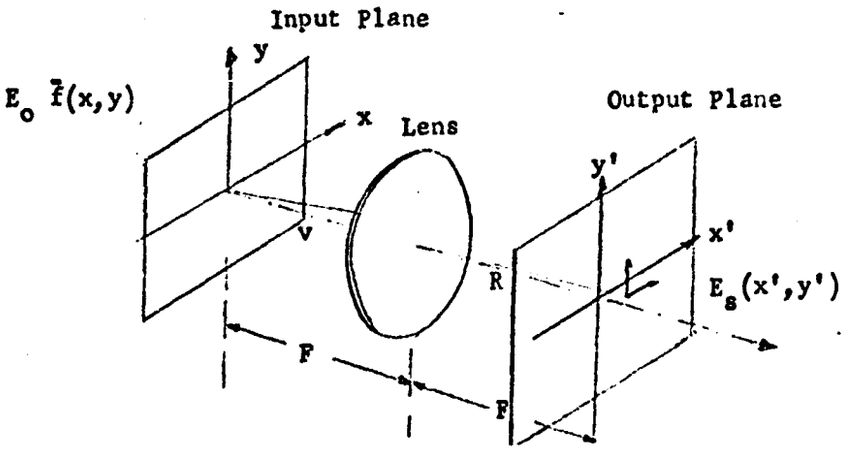

FIG. 23 - FOURIER TRANSFORMATION OF SIGNAL LIGHT DISTRIBUTION

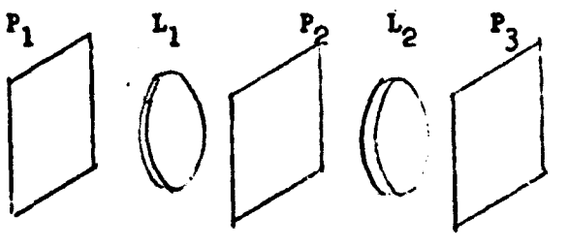

FIG. 24 - TWO-LENS SYSTEM FOR FILTERING AND REPRODUCTION OF SIGNAL LIGHT DISTRIBUTION

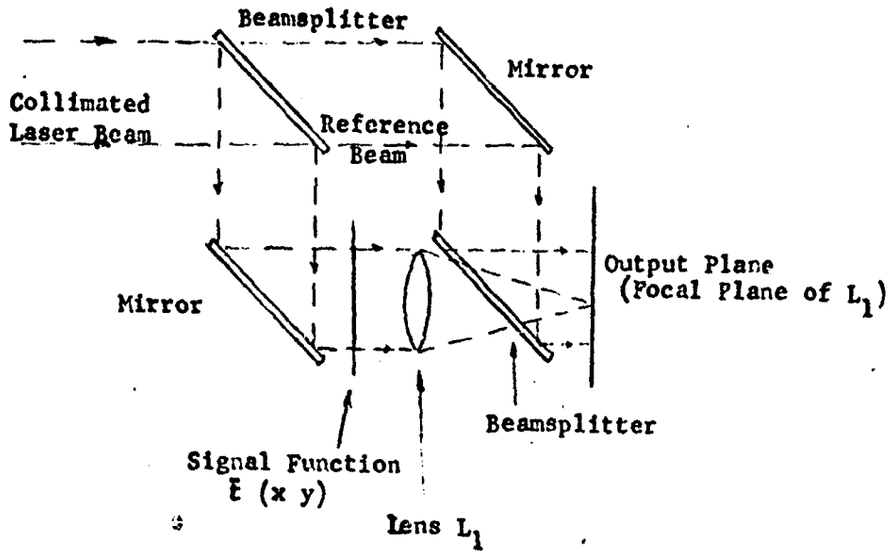

FIG. 25 - PREPARATION OF COMPLEX MATCHED FILTER TRANSPARENCY

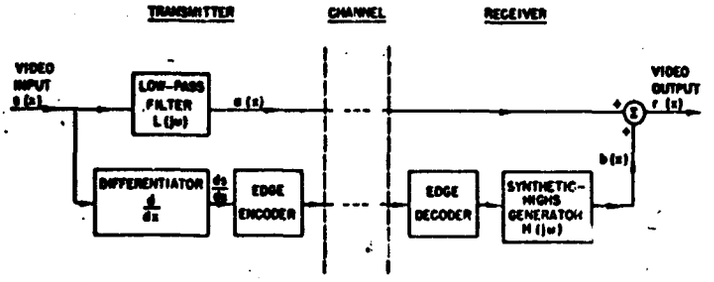

FIG. 26 - EDGE-ENHANCEMENT SYSTEM (1-dimension)
(Reference 16)

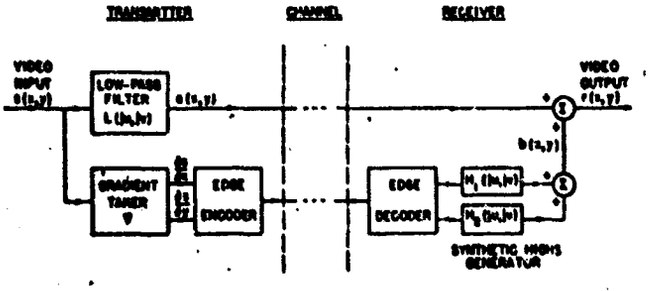

FIG. 27 - TWO-DIMENSIONAL EDGE-ENHANCEMENT SYSTEM
(Reference 16)

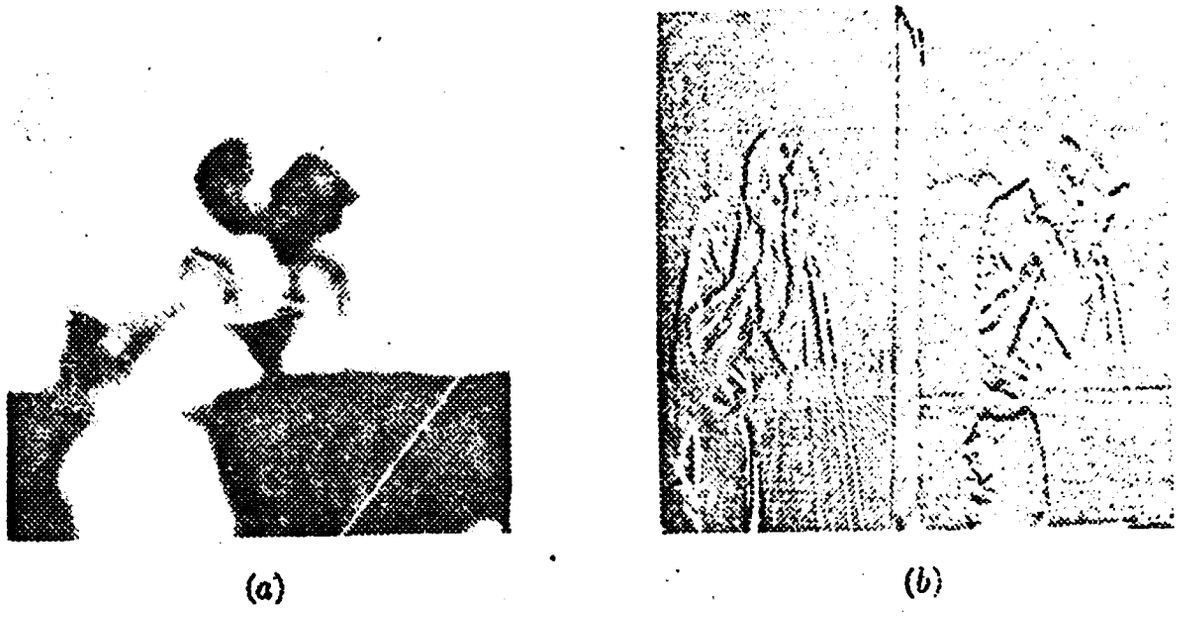

(a) (b)

(c) (d)

FIG. 28 - EXAMPLE OF TWO-DIMENSIONAL EDGE-ENHANCEMENT PROCESS (Ref. 13)

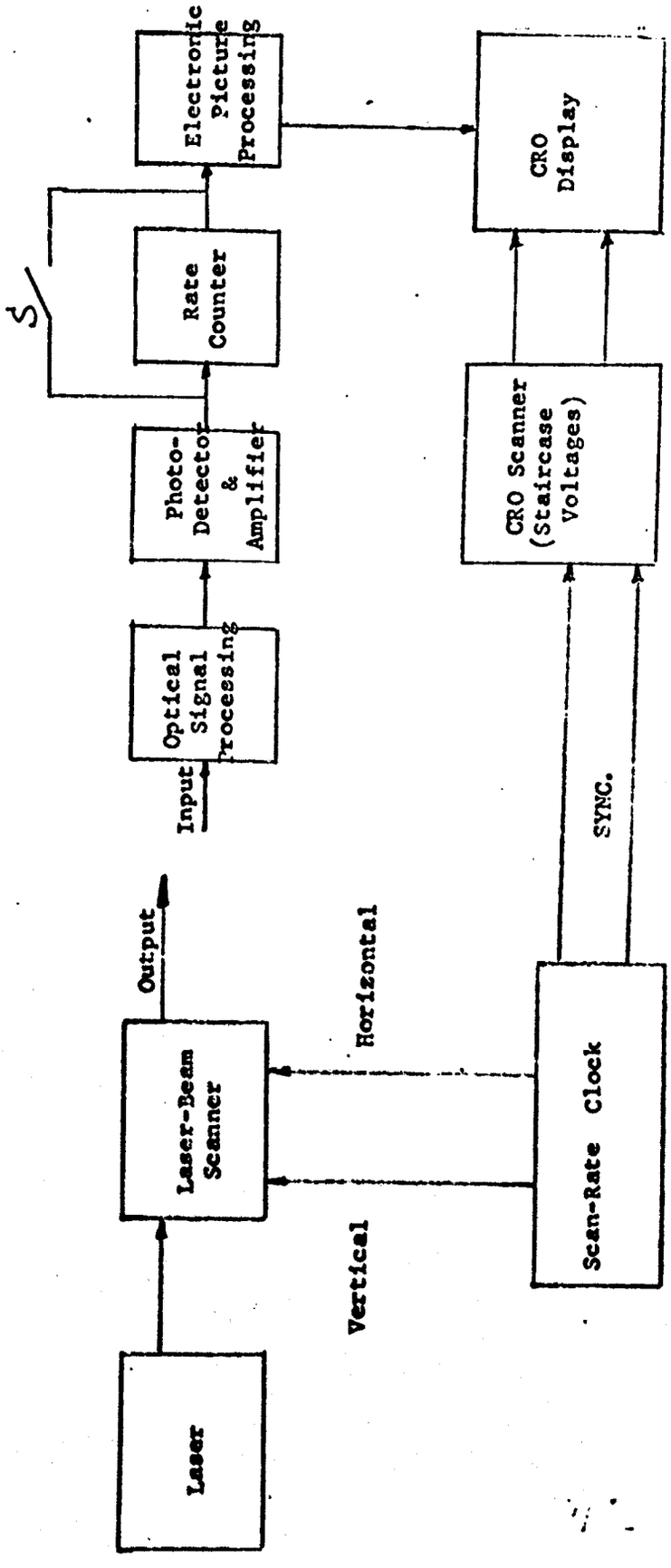

FIG. 29 - BLOCK DIAGRAM OF LASER OPTICAL SIGNATURE DETECTION SYSTEM

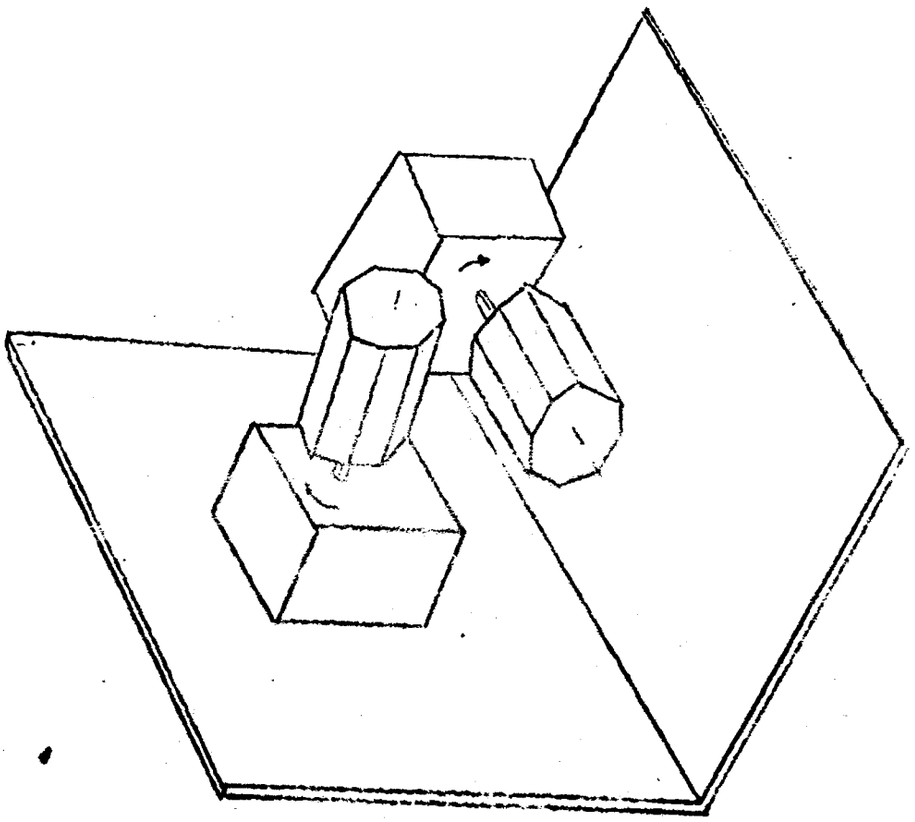

FIG. 30 - SKETCH OF TWO-DIMENSIONAL MECHANICAL SCANNER

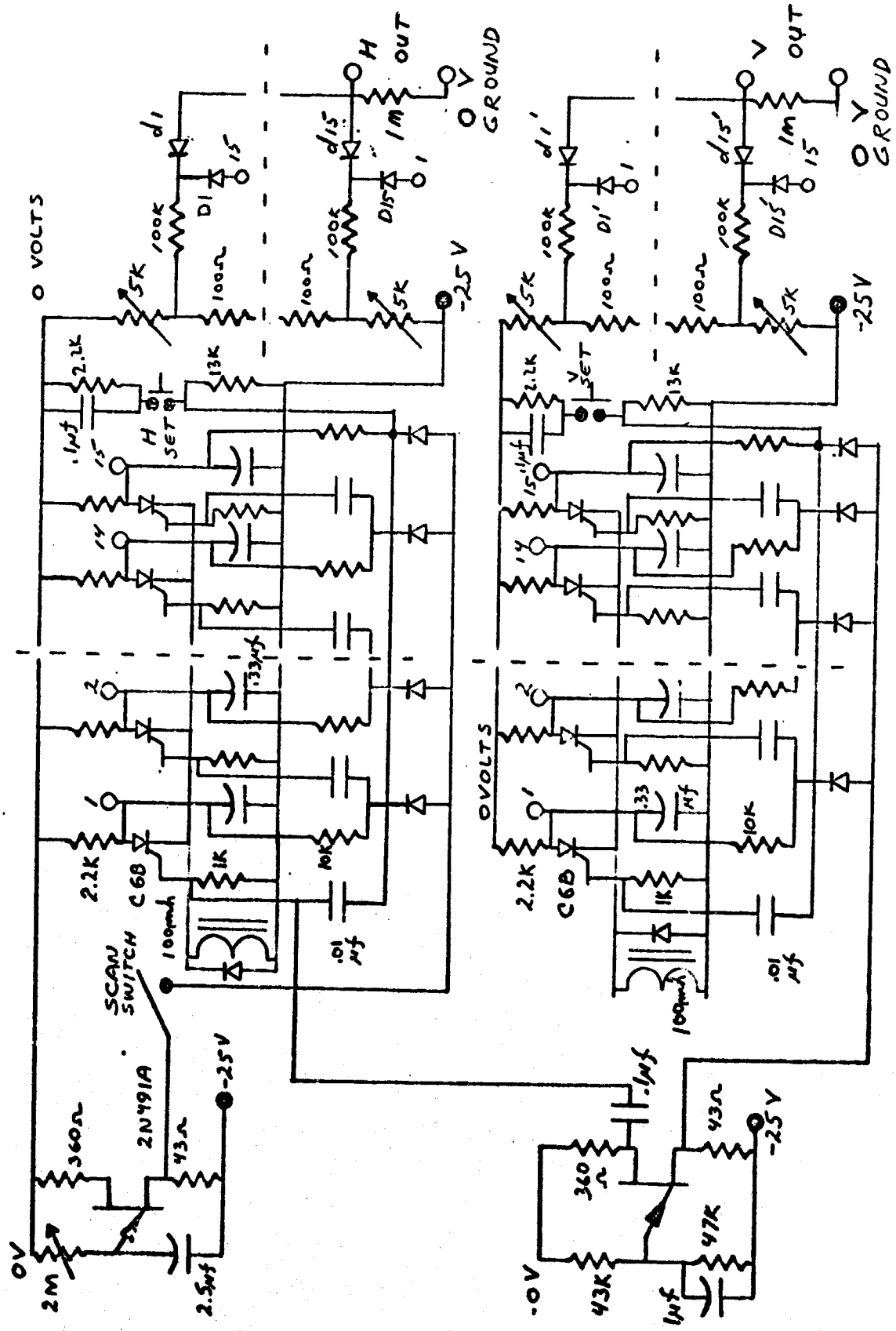

FIG. 31 - STAIRCASE VOLTAGE GENERATOR AND RATE CLOCK

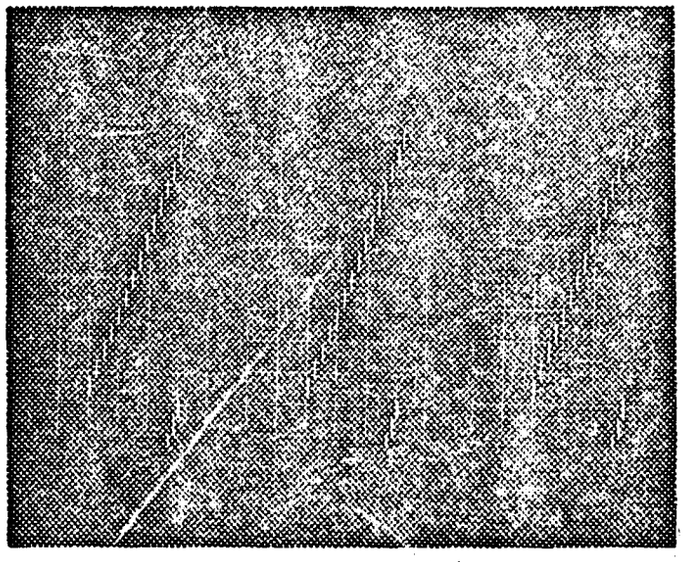

FIG. 32 - STAIRCASE VOLTAGE WAVEFORM

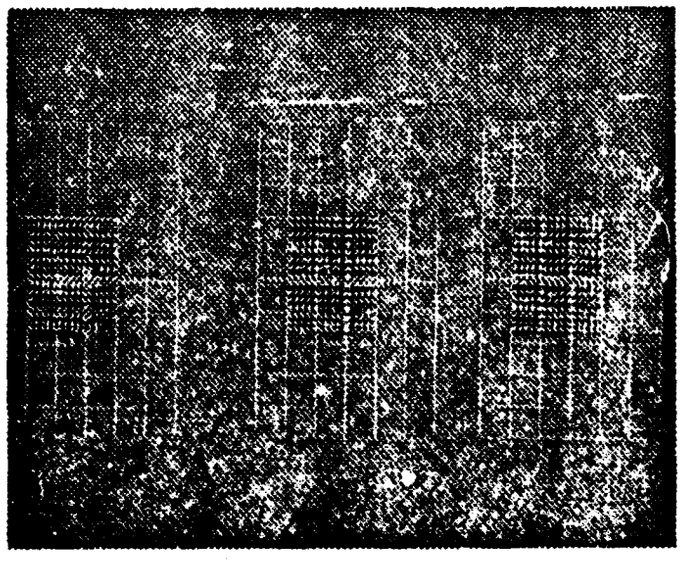

FIG. 33 - MATRIX DISPLAY (15 x 15)

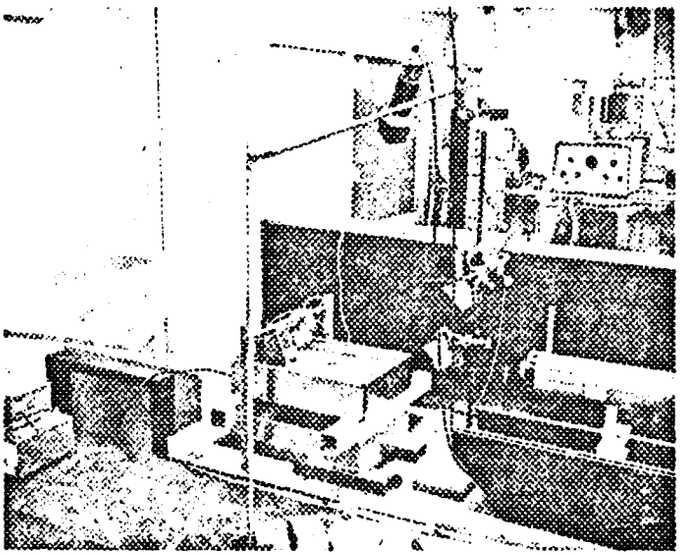

FIG. 34 - LASER, MECHANICAL SCANNER, BENCH WATER TANK WITH WAVE MAKER. Also, a Photomultiplier and a Fresnel Lens Collector are shown.

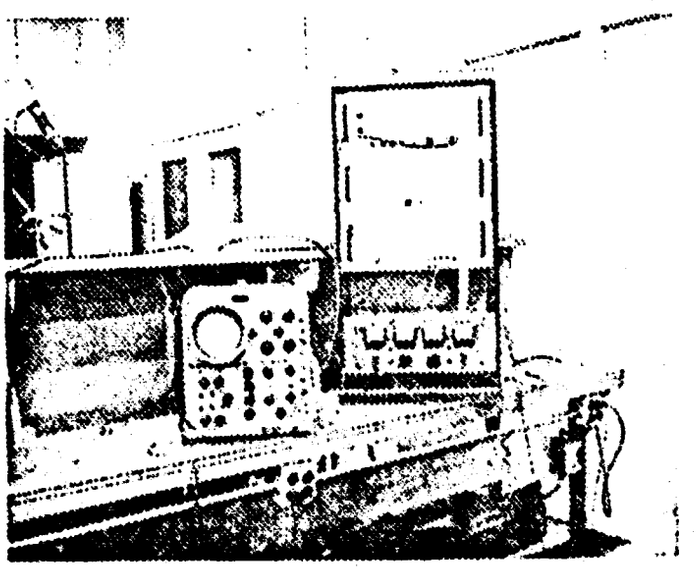

FIG. 35 - RACK-MOUNTED EQUIPMENT (RATE CLOCK, STAIRCASE GENERATOR, AMPLIFIER, RATE COUNTER, POWER SUPPLY) AND DISPLAY SCOPE.

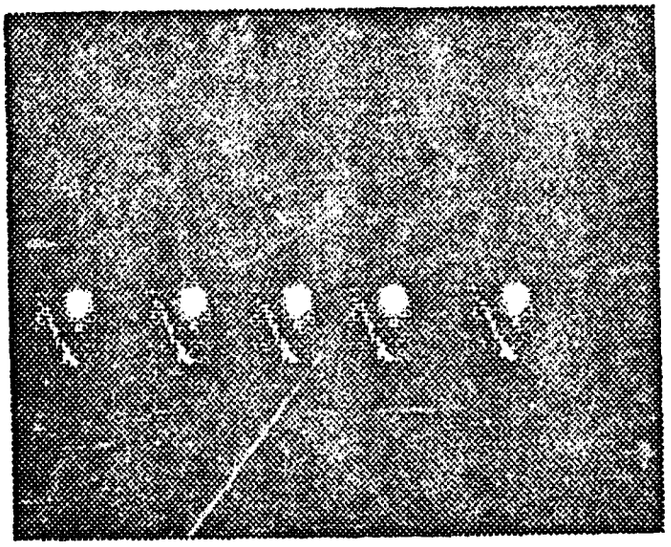

a)

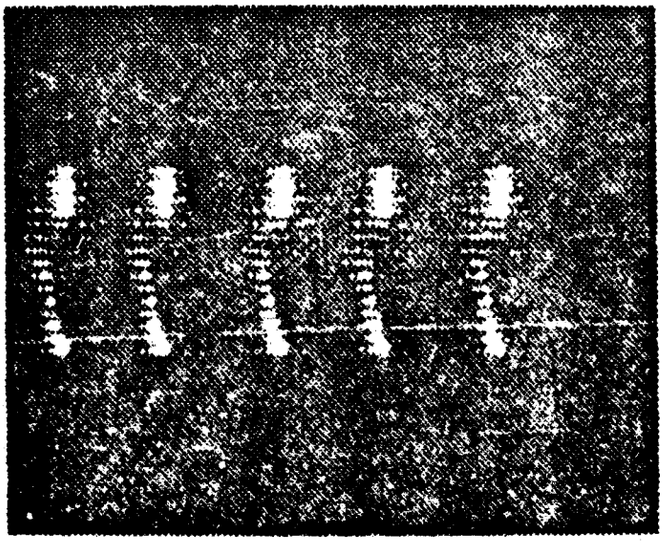

b)

FIG. 36 - EXAMPLES OF PATTERN DISPLAY

a) Rectangular Display
b) Expanded Horizontal Dimension

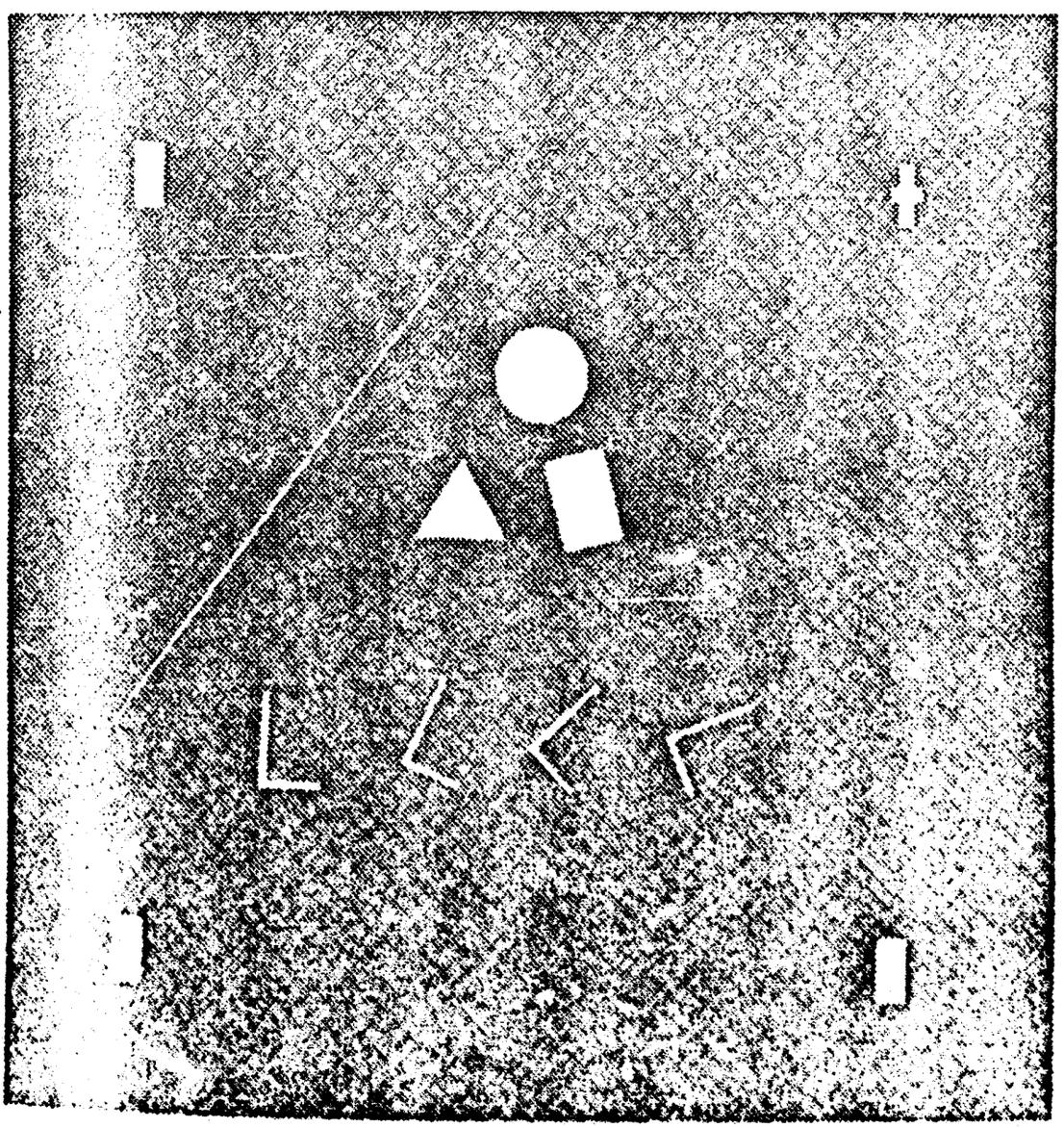

(a)

FIG. 37 - EXAMPLES OF SIGNALS WITH VARIOUS GEOMETRIC PATTERNS (Ref. 12)

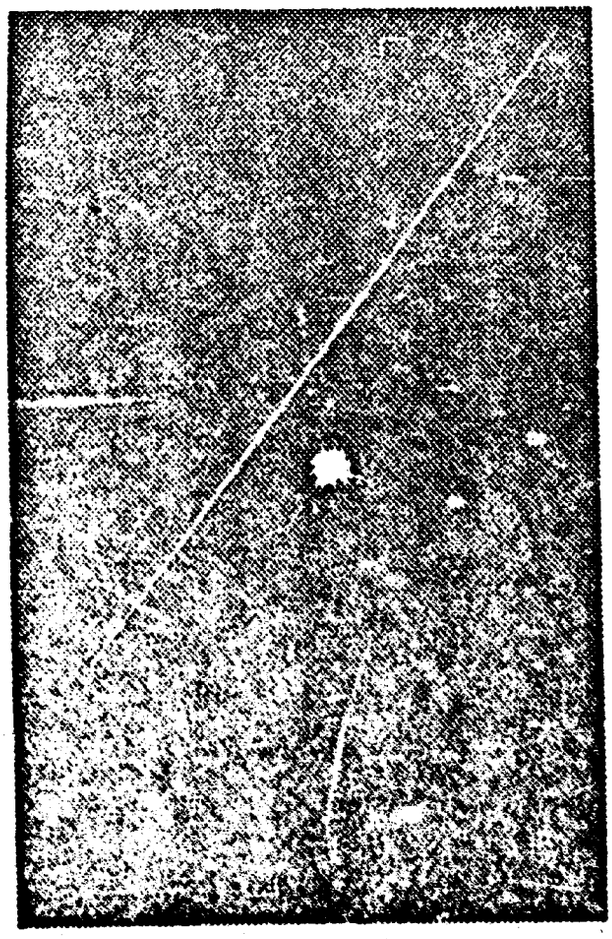

FIG. 38 - COMPLEX FOURIER TRANSFORM OF L-PATTERN (Ref. 12)

FIG. 39 - CROSS-CORRELATION OF L-MASK WITH INPUT SIGNALS OF Fig. 37